The Detectability and Constraints of Biosignature Gasses in the Near & Mid-Infrared from Transit Transmission Spectroscopy

by

Luke Tremblay

A Thesis Presented in Partial Fulfillment
of the Requirements for the Degree
Master of Science

Approved November 2019 by the
Graduate Supervisory Committee:

Michael Line, Chair
Evgenya Schkolnik
Sara Walker

ARIZONA STATE UNIVERSITY

December 2019

ABSTRACT

The James Webb Space Telescope (*JWST*) is expected to revolutionize the current understanding of Jovian worlds over the coming decade. However, as the field pushes towards characterizing cooler, smaller, "terrestrial-like" planets, dedicated next-generation facilities will be required to tease out the small spectral signatures indicative of biological activity. Here, the feasibility of determining atmospheric properties, from near to mid-infrared transmission spectra, of transiting temperate terrestrial M-dwarf companions, has been evaluated. Specifically, atmospheric retrievals were utilized to explore the trade space between spectral resolution, wavelength coverage, and signal-to-noise on the ability to both detect molecular species and constrain their abundances. Increasing spectral resolution beyond R=100 for near-infrared wavelengths, shorter than 5μm, proves to reduce the degeneracy between spectral features of different molecules and thus greatly benefits the abundance constraints. However, this benefit is greatly diminished beyond 5μm as any overlap between broad features in the mid-infrared does not deconvolve with higher resolutions. Additionally, the inclusion of features beyond 11μm did not meaningfully improve the detection significance nor abundance constraints results. The findings of this study indicate that an instrument with continuous wavelength coverage from approximately 2-11μm and with a resolution of R$\simeq$50-300, would be capable of detecting H_2O, CO_2, CH_4, O_3, and N_2O in the atmosphere of an Earth-analog transiting an M-dwarf (mag_K=8.0) within 50 transits, and obtain better than an order-of-magnitude constraint on each of their abundances.

The Origins Space Telescope (*Origins*) is one of four flagship mission concepts, under review by the 2020 Decadal Survey, that may take the mantle of the next-generation space-based observatory. In conjunction with this research, a secondary trade space study was performed on behalf of the Origins Exoplanets Working Group.

The primary purpose of this collaboration was to provide a scientific basis to the technical specifications for the mid-infrared detectors onboard the Mid-Infrared Spectrometer Camera Transit Spectrometer (MISC-T) instrument. The results of this work directly contributed to the alteration of the official technical specifications of the instrument design concept.

DEDICATION

With the final word of this publication, the following work marks the closing of a defining chapter in my life. To my advisor Michael Line, I thank for the unrivaled amount of support and understanding he has provided for the past two and half years. To my fellow students and colleagues, I appreciate the struggles and successes you have shared alongside me in our academic endeavors. To my mother and father, I offer an immeasurable amount of thanks for your enduring support, your infinite love, and the privileges which have provided me with the opportunities to achieve. Perhaps most importantly though, I thank you both for your stern hands that have helped mold me into the man I am today, capable and confident in overcoming life's most trying moments. And lastly, to the person I eagerly wish to start the next chapter of my life with, my greatest supporter, my exceptional source of encouragement, and the love of my life; I dedicate this thesis.

TABLE OF CONTENTS

LIST OF TABLES

LIST OF FIGURES

Chapter 1

INTRODUCTION

Characterizing the climate and composition of terrestrial atmospheres is a primary goal of exoplanet science over the next few decades (NAS 2020 Vision[1]). Among the growing catalog of targets, *temperate terrestrial* exoplanets are of great interest due to their possible astrobiological implications. Namely, their potential to develop and maintain volatile-rich secondary atmospheres capable of supporting biology. As Earth is the only known planet to host life, it is straight-forward that we would begin our search for extraterrestrial life by considering the conditions on Earth as the primary conditions which must exist for the development of life as we know it.

The principal gases that comprise Earth's atmosphere (nitrogen/nitrous oxide, water, carbon dioxide, oxygen/ozone, and methane) are generally regarded as "bio-indicators" meaning that their presence is indicative of potentially habitable atmospheric conditions. "Biosignatures" are those observables that are representative of biological processes affecting the planet's atmospheric chemistry (i.e. the presence of life). Catling and Kasting (2007) showed that all of the bulk gases in Earth's atmosphere, excluding inert gases, are influenced by biogenic processes. Life on Earth is the primary contributor to the global chemical disequilibrium (Krissansen-Totten et al. 2016), and for this reason disequilibrium is presumed to be a robust biosignature (Cockell et al. 2009, Kasting et al. 2009, Léger 2000, Sagan et al. 1993, Seager 2014, Seager & Bains 2015, Seager & Deming 2010). The combinations of molecules responsible for Earth's disequilibrium are O_3+CH_4 and O_3+N_2O (Krissansen-Totten et al. 2016). If detected at certain abundances, the presence of these molecules si-

[1]https://sites.nationalacademies.org/cs/groups/bpasite/documents/webpage/bpa_064932.pdf

multaneously cannot be plausibly explained by abiotic processes (Domagal-Goldman et al. 2014; Harman et al. 2015; Leger et al. 1993; Meadows et al. 2018b; Segura et al. 2003; Tian et al. 2014; Schwieterman et al. 2016; Meadows 2017; Harman & Domagal-Goldman 2018). As such, a key goal of exoplanet exploration is to detect the presence and quantify the abundances of these gases on nearby terrestrial worlds.

Due to the favorable planet-to-star radius ratio and occurrence rates, M-dwarf systems offer the most promising near-term opportunity for characterizing temperate terrestrial worlds and the possible presence of biosignatures. Ground-based radial velocity surveys and the Transiting Exoplanet Survey Satellite (*TESS*) are expected to detect dozens of temperate terrestrial-sized (0.8 - 1.6$R_{\oplus}$) exoplanets around M-dwarf's (Quirrenbach et al. 2018; Barclay+2018; Kempton+2018; Zechmeister et al. 2019), potentially amenable to follow-up with *JWST* over the coming decade. Numerous previous works have demonstrated that *JWST* will likely provide astounding constraints on the atmospheric properties of Jovian-to-Super-Earth planets (Deming et al. 2009, Beichman et al. 2014, Barstow et al. 2014, Greene et al. 2016, Batalha & Line 2017; Rocchetto et al. 2016; Benneke & Seager 2013). However, it remains an open question as to how well *JWST* will perform as it is pushed to observe temperate terrestrial bodies with smaller spectral features. Possible limitations may stem from a combination of large detector noise floors (similar detector technology as *HST* WFC3 and *Spitzer* IRAC, Greene et al. 2016), saturation limits for the brightest targets (Batalha et al. 2018), and lack of continuous near-to-mid-infrared wavelength coverage in a single mode (greatly increasing the number of required transits).

The discovery of the TRAPPIST-1 system (Gillon et al. 2016, 2017) has lead to a number of works investigating the climate, composition, and internal structure of temperate M-dwarf worlds (Unterborn et al. 2017; Turbet et al. 2018; Suissa & Kipping 2018; Meadows et al. 2017; Wunderlick et al. 2019). Complementary to these

efforts, recent studies have explored the capabilities of *JWST* to characterize various atmospheric compositions on TRAPPIST-1 planets through both transmission and thermal emission spectroscopy (Barstow & Irwin 2016; Morley et al. 2017; Batalha et al. 2018; Krissansen-Totten et al. 2018; Lustig-Yaeger et al. 2019; Wunderlick et al. 2019).

Morley et al. (2017) concluded that *JWST*'s NIRSpec G235M/F170LP mode (1.66 - 3.07μm) would be capable of rejecting a flat-line spectrum at 5σ confidence within 20 transits for a range of atmospheric compositions. While a flat-line rejection test is valuable, it does not guarantee the ability to detect the presence of any specific molecule with high statistical confidence. Lustig-Yaeger et al. (2019) concluded that transmission spectroscopy with NIRSpec PRISM is optimal for detecting the presence of high mean molecular weight atmospheres within $\sim$12 transits. Additionally, they find that CO_2, if present, will be easily detectable regardless of the atmospheric composition and MIRI-LRS may be capable of detecting the 9.6μm O_3 feature on planet 1e (with an SNR=3) with greater than 100 transits (exceeding the number of observable transits in the mission lifetime). Wunderlich et al. (2019) produced self-consistent forward models for the atmosphere of an Earth-like planet around early-to-late M-dwarfs. Their "Earth around TRAPPIST-1" model notably predicts a greatly increased temperature in the mid-to-upper atmosphere, inflating the scale height and increasing the detectability of molecular species through transmission spectroscopy. Furthermore, the predicted chemical evolution indicated a significant enhancement of CH_4 and H_2O compared to modern Earth and subsequently, that their corresponding spectral features, along with CO_2, would be detectable within $\sim$10 transits when using the appropriate NIRSpec high-resolution filters.

Barstow & Irwin (2016) performed a retrieval analysis on synthetic spectra of the inner-most TRAPPIST-1 companions (b, c, d) each with an Earth-like composition

atmosphere. Utilizing a combination of NIRSpec PRISM and MIRI-LRS, they concluded that O_3, at Earth-like abundances, would be detectable on planets 1c and 1d with 30 transits on each instrument. Utilizing an atmospheric retrieval analysis, Krissansen-Totten et al. (2018) analyzed the detectability of the CO_2+CH_4 disequilibrium biosignature, suspected to have been present in Earth's early (Archean) atmosphere when the abundances of each were significantly enhanced compared to modern-day values. They concluded that *JWST* would be capable of obtaining order-of-magnitude constraints on the mixing ratios of both CH_4 and CO_2 in an Archean Earth-like atmosphere, in $\sim$10 transits. Alternatively, the abundance of O_3 in a modern Earth-like atmosphere could not be constrained by NIRSpec Prism and would be completely unbounded by MIRI-LRS.

While it may be possible for *JWST* to detect and constrain the dominant molecular species in certain terrestrial atmospheres with advantageous compositions, existing literature does not substantiate its capabilities to detect or constrain the abundances of the five primary bio-indicators in a modern Earth-like atmosphere on a terrestrial M-dwarf companion.

The primary aims of the following studies was to develop a baseline understanding of how key observational parameters (spectral resolution, wavelength coverage, and signal-to-noise) of near-to-mid-infrared transmission spectra influence the ability to detect and constrain biologically relevant molecular species in the atmospheres of transiting Earth-like planets orbiting M-dwarfs. We leveraged powerful Bayesian retrieval tools to obtain both parameter constraints and Bayesian molecular detection significances as a function of the instrumental trades. Chapter 2 details the setup for our forwards model and retrieval techniques. Chapter 3 describes the instrumental-trade space that we explored. Chapter 4 summarizes the key results followed by a discussion and key points in Chapter 5.

Chapter 2

SIMULATION SET-UP

Here, we outline the development of our forward model used to compute the synthetic transmission spectra, elaborate on the instrumental trade space, discuss the details of our instrument noise model, and review our retrieval approach.

2.1 Transmission Forwards Model

We simulate the transmission spectrum of a terrestrial planet, with mass and radius equivalent to TRAPPIST-1e, residing within the "habitable zone" of TRAPPIST-1 with an approximate modern Earth-like atmosphere (observational system setup/ signal-to-noise discussed below). We acknowledge, up front, that this may not be a physically plausible scenario due to the vastly different incident spectral energy distribution. However, given the overwhelming number of unknowns involved in self-consistent planetary atmosphere modeling (e.g., star-planet interactions, surface fluxes, formation conditions, bulk elemental composition, 3D atmospheric dynamical effects, cloud micro-physics, dynamical evolution/history) we simply choose to treat our atmosphere as "Earth-like" (as has also been done in previous works, Morley et al. 2017; Krissansen-Totten et al. 2018).

To produce model transmission spectra, we leverage a variant of the CHIMERA[1] transmission spectrum routine (Batalha & Line 2017; Line et al. 2013; Greene et al. 2016; Line & Parmentier 2016). Specifically, we re-parameterize the code (Table 2.1) to make it more amenable for temperate worlds by including as free parameters the constant-with-altitude mixing ratios of H_2O, CO_2, CO, CH_4, O_3, N_2O and

[1] https://github.com/ExoCTK/chimera

an "unknown" background gas with a free-parameter molecular weight (taken to be earth's N_2+O_2 value), an isothermal "scale-height" temperature, planetary radius at the surface (or scaling there-of), and an opaque gray cloud-top-pressure (nominal truth values given in Table 2.1). We mimic refraction with this cloud top pressure (here, 0.56 bars) using the prescription from Robinson et al. (2017), but otherwise assume a cloud free atmosphere (the refractive layer is in affect, mimicking a cloud, as well as its inclusion as a free parameter). CHIMERA uses correlated-K opacities (computed at the given constant resolving powers below), here derived from a grid of pre-computed line-by-line ($\leq$0.01 cm^{-1}, 70 - 410K, 1E-7 - 30 bar) cross-sections generated with the HITRAN HAPI Routine (Kochanov et al. 2016) and the HITRAN2016 line database (Gordon et al. 2016). We do not include collision induced opacities, though they may spectrally present themselves (Schwieterman et al. 2015).

2.2 Parameter Estimation & Model Selection Approach

We perform Bayesian parameter estimation and model selection, on the simulated datasets described below, using the pyMultiNest routine (Buchner et al. 2014) following the methods described in Benneke & Seager (2013). We initialized our retrievals with 3000 live points. An advantage of nested sampling algorithms is ease of evidence computation, which can be used to assess model complexity. We use Bayesian nested model comparison (by removing one gas at a time) to determine the detection significance of each molecular species (Trotta 2008; Benneke & Seager 2013), and is what we utilize as a metric for assessing instrument performance. An advantage of utilizing the detection significance via the Bayesian evidence, over more traditional methods (e.g., "line" or "band" height above a continuum relative to the noise) is that it fully utilizes all of the spectral information included in all of the relevant bands as well as encompasses the model degeneracies.

2.3 Simulated Spectrograph & Radiometric Noise Model

The noise model used for this study is adapted from Greene et al. (2016) for characterizing transiting exoplanet atmospheres with *JWST*. The software package computes a realistic transmission spectrum (including uncertainties) of an exoplanet passing in front of a model star. The code also takes as input the limiting fractional precision (i.e. noise floor) of the instrument.

Modifications were made to the code to reflect the expected performance of a next-generation mid-infrared telescope with a 25m^2 collecting area, 3 arcsec radius field aperture, 2.85 - 30 micron wavelength range (HgCdTe detectors below 10.5 microns and SiAs detectors above 10.5 microns), a zodiacal background estimated by Glass et al. (2015a, 2015b), and an intrinsic resolving power of 300. These modifications reflect the capabilities of new detector technologies discussed by Matsuo et al. (2018).

Our input stellar spectrum derives from the PHOENIX stellar models using the PySynPhot software package (Husser et al. 2013). We adopted the values for TRAPPIST-1 (T=2550K, M/H=0.40, $\log(g)$=4.0) and stellar radius of 81373.5km from Gillion et al. (2016). Additionally, we have scaled the stellar spectrum to a K-band magnitude of 8.0 rather than $\text{mag}_K = 10.3$, TRAPPIST-1's native magnitude. While this may be representative of an optimistic scenario, $\text{mag}_K = 8.0$ is the mean magnitude of the brightest 10 M-dwarf stars in the Barclay catalog of the predicted *TESS* yield (Barclay et al. 2018).

	Model Value	Uniform Prior
$\log(H_2O)$	-5.5	[-12, 0]
$\log(CO_2)$	-3.45	[-12, 0]
$\log(CH_4)$	-6.3	[-12, 0]
$\log(O_3)$	-6.5	[-12, 0]
$\log(N_2O)$	-6.3	[-12, 0]
log(CO)	-7.0	[-12, 0]
T_{iso}	280K	[100, 800]
xR_P	$0.918R_\oplus$	[0.5, 1.5]
log(CTP)	-0.25	[-6, 2]
Bkg MMW	28.6	[2.0, 44.0]

Table 2.1: The 10 free parameters, the model values, and their associated uniform priors used in our CHIMERA radiative transfer and retrieval code.

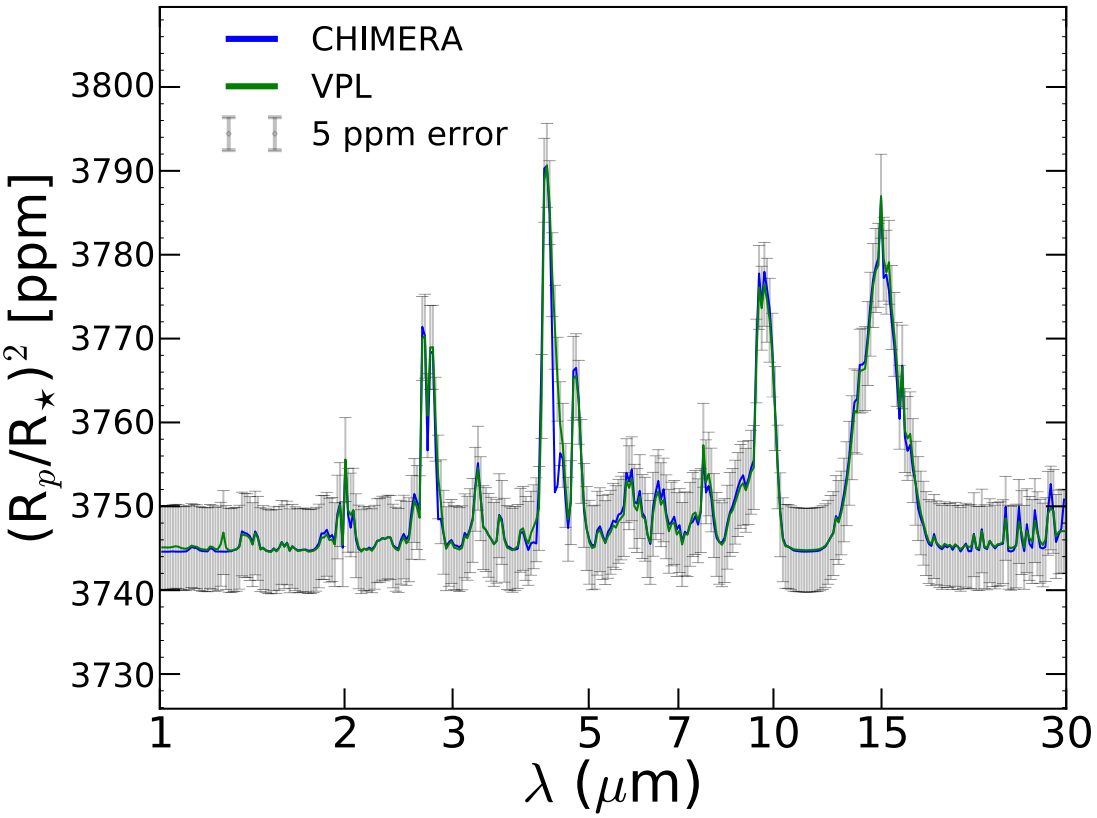

Figure 2.1: Validation of our transmission forward model (at R=100) against the Virtual Planetary Laboratory (VPL) Earth model[2] utilizing the same temperature-pressure and gas mixing ratio profiles. The spectra were scaled to a $1R_\oplus$ around a $0.15R_\odot$ star. For reference, overlaid are 5 ppm error bars.
[2](*http://depts.washington.edu/naivpl/content/vpl-spectral-explorer)*

Short Wavelength Boundary	Long Wavelength Boundary	Spectral Resolution
1μm	5μm	300
		100
		50
	11μm	100
		50
	30μm	100
		50
		30
3μm	5μm	300
		100
		50
	11μm	300
		100
		50
	30μm	100
		50
		30
5μm	11μm	100
		50
		30
	30μm	100
		50
		30

Table 2.2: A breakdown of the 23 test cases evaluated in this study as a combination of wavelength coverage and spectral resolution.

Chapter 3

OBSERVATIONAL PARAMETER SPACE

We produce synthetic transmission spectra of our Earth-like atmosphere model over a grid of spectral resolution and bandpass choices. The nominal wavelength coverage was chosen to cover the near and mid-infrared regimes spanning 1-30μm, shown in Figure 3.1. We divide this wavelength range into 8 separate regimes to explore the influence of additional bands of a given molecule and their overlap with features of other molecules. Additionally, we test low and moderate spectral resolutions ranging from R=30 to R=300. The spectral resolution ($\lambda/\delta\lambda$) dictates the degree to which individual molecular bands can be resolved and overlap degeneracies broken. Figure 3.2 compares the spectra at the resolutions explored in this work. We simulate different resolutions within each spectral band in order to explore the resolution trade along with each wavelength regime. This produces a grid of 23 test cases (shown in Table 2.2) to evaluate through our retrieval algorithm described in 2.2.

In addition to resolution and wavelength coverage, we also explored the signal-to-noise trade, parameterized here as the number of transits (1-100), which can be considered a proxy for mirror diameter or source magnitude, where the noise on a single transit is defined by the "nominal" noise model setup described in 2.3. Utilizing this trade, we explored the minimum number of transits necessary to achieve a threshold 3.6σ confidence level detection of each molecule. We provide Equations 3.1 & 3.2 as a means of converting our retrieval results to stars of differing magnitudes or for different sized collecting mirrors.

$$M_{eff} = 8.0 - 2.5 \log_{10}(\frac{T_2}{T_1}) \tag{3.1}$$

Where T_2/T_1 is the ratio determining how many more or less transits are equivalent to a change from the native magnitude ($M_{nom} = 8.0$) to a new magnitude (M_{eff}).

$$A_{eff} = 25\sqrt{\frac{T_2}{T_1}} \tag{3.2}$$

Where T_2/T_1 is the ratio determining how many more or less transits are equivalent to a change from the native collecting area ($A_{nom} = 25\text{m}^2$) to a new mirror size (A_{eff}).

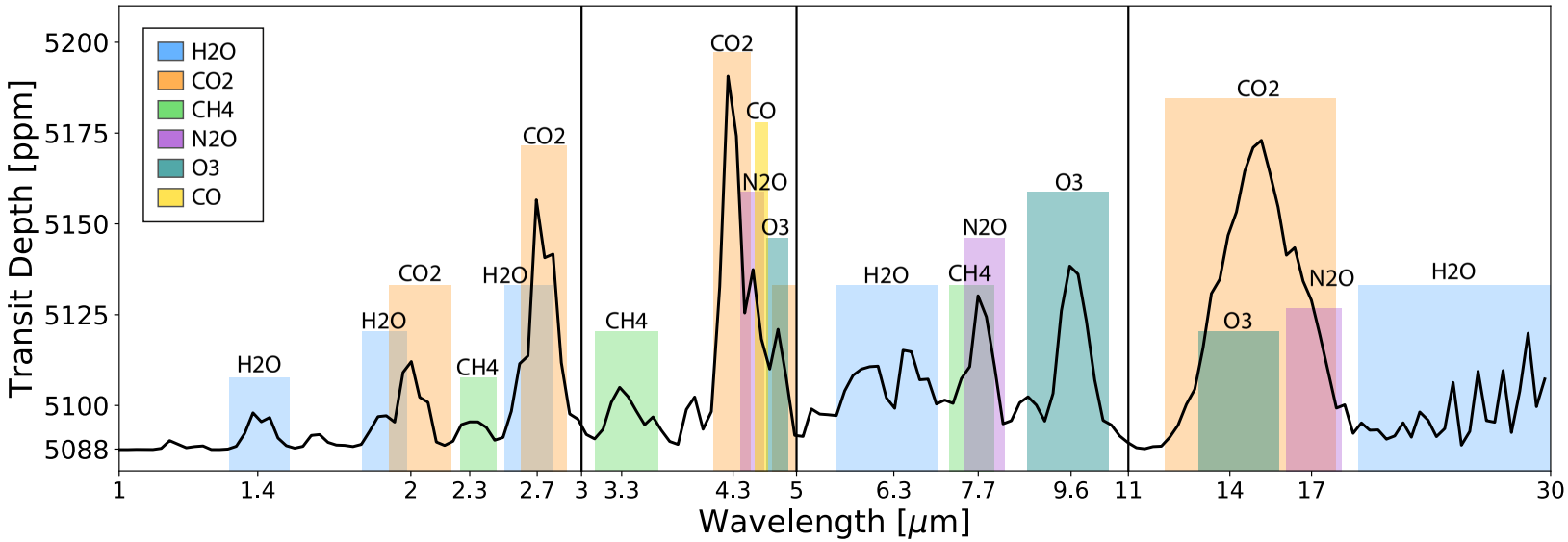

Figure 3.1: Wavelength region explored in this work (here, shown at R=50). The colored bands indicate the presence, and approximate width, of a spectral feature for a given molecule. We explore constraints obtainable over several wavelength bands within this region (Table 2.2).

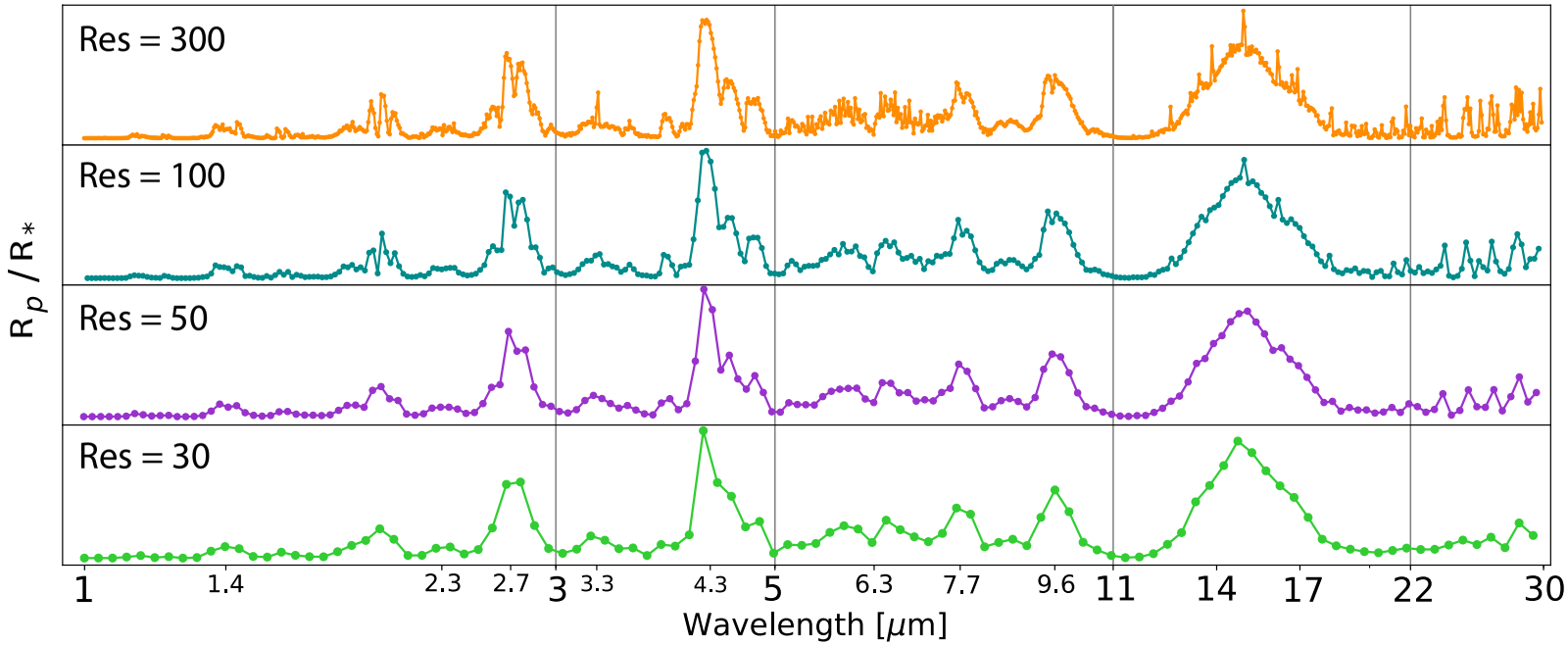

Figure 3.2: Influence of resolution on spectral features. Lower resolution results in the blending of features, causing a loss of information. The vertical lines at 3, 5, and 11μm denote the division of the wavelength regimes explored in this study.

Chapter 4

RETRIEVAL RESULTS

For the majority of our test cases, the inclusion of a broader bandpass decreases both the necessary observation time to claim a statistically significant detection and reduces the uncertainty on the abundance constraints. Therefore, with few molecule-specific exceptions, we find that altering the choice of wavelength coverage has a more prominent benefit for both our detection significance values and abundance constraints than the choice of spectral resolution. Tables 4.1 & 4.2 provide all of our retrieval results for detection significance and abundance constraints, respectively. Figure 4.1 visually summarizes these results for four key bandpasses (1-5μm, 1-11μm, 3-11μm, and 5-30μm) over each of the spectral resolutions probed for those bandpasses. Figure 4.2 provides a visual understanding of how the abundance constraints, for each molecular species, become narrower as a function of the signal-to-noise trade by increasing the number of transits observed.

Our detection significance analysis directly compares each bandpass and resolution combination by determining the number of transits required to achieve a 3.6σ detection for a specific molecule. Table 4.1 displays these required number of transits for each molecule over each combination of resolution and wavelength coverage.

Table 4.2 enumerates the 1σ error widths for each molecule within each of our 23 test cases at 50 transits. Figures 4.3 through 4.7 within each of the following sections reveal the influence that an increasing number of transits has on the abundance constraints, for each molecule individually at R=100. The following subsections provide an in-depth analysis of each molecule and the most relevant transitions that influence our abundance constraints and detection significance results.

4.1 Water (H_2O)

Water has spectral features spanning nearly the entire wavelength range in this study, with the most prominent features centered at 2.65μm and 6.3μm. Additionally, there are two smaller features extending into the near-infrared at 1.4μm and 1.85μm as well as a series of features upwards of 20μm. The most relevant comparison is between the near-infrared (which we define as the 1-5μm bandpass) and the mid-infrared (5-11μm). In isolation from other water features in the 5-11μm region, the broad 6.3μm feature produces comparatively underwhelming results (for both detection significance and abundance constraints) likely due to the limited contribution from the few other prominent features in this bandpass (Benneke & Seager 2012). In contrast, the 1-5μm region encompasses the prominent 2.65μm feature as well as the two smaller features. The precision on the abundance constraints improves by approximately 60% both when increasing the resolution from R=50 to R=100 and again from R=100 to R=300. However, it is worth noting that these near-infrared features are very narrow and are thus significantly more sensitive to changes in the choice of spectral resolution. High resolution values will deconvolve overlapping spectral features of different molecular species. At a resolution of R=100, a single H_2O feature in the near-infrared consists of between 10-20 resolution elements compared to 44 for the 6.3μm feature.

While the near-infrared (1-5μm bandpass) produces the tightest abundance constraints, it does not provide the greatest detection significance values given the same spectral resolution and number of transits. By comparison, the 3-11μm range (which does not include additional H_2O features) requires 33.9% less observation time at R=100 and 50.0% less at R=50 than the 1-5μm bandpass. Alternatively, by looking further into the mid-infrared, the 5-30μm bandpass offers a 3.4% decrease at R=100 and a 24.5% decrease at R=50 compared to the 1-5μm bandpass.

4.2 Carbon Dioxide (CO_2)

Due to its prominent spectral features across most of the near and mid-infrared, CO_2 is the easiest molecule to detect within each of our bandpass choices, with the exception of 5-11μm. CO_2 possess four prominent spectral features centered at 2.0, 2.7, 4.3, and 15um. The 5-11μm region is the only bandpass choice which does not include a spectral feature for CO_2. Any other choice of wavelength coverage and spectral resolution evaluated in our study proved to be sufficient to constrain CO_2 in less than 7 transits. The inclusion of the 4.3μm feature ensures a 3.6σ detection within the observation time of approximately a single transit.

Despite the strong detection of CO_2, the abundance constraints are ironically, not as precise as would be expected. This is largely due to the fact that deriving narrow abundance constraints relies on a change in the strengths of the spectral features. Line & Parmentier (2016) derive the function for spectral modulation with respect to wavelength for multiple absorbing molecular species, reproduced here for convenience (Equation 4.1).

$$\frac{d\alpha_\lambda}{d\lambda} = \frac{2R_p}{R_\star^2} H \frac{1}{1+\frac{\xi_2\sigma_{\lambda,2}}{\xi_1\sigma_{\lambda,1}}} \left(\frac{d\ln(\sigma_{\lambda,1})}{d\lambda} + \frac{\xi_2\sigma_{\lambda,2}}{\xi_1\sigma_{\lambda,1}} \frac{d\ln(\sigma_{\lambda,2})}{d\lambda} \right) \tag{4.1}$$

Where $d\alpha_\lambda/d\lambda$ is the wavelength dependent slope of the transmission spectra. H is the scale height given by $\frac{k_b T}{\mu g}$ and $\sigma_{\lambda,i}$ and ξ_i are the absorption cross section and abundance, respectively, of a given molecular species.

In the case of CO_2, the $\xi_1\sigma_{\lambda,1}$ term is so much greater than the other absorbers that the spectral modulation due to CO_2 becomes insensitive to even large changes in the abundance. The retrieval thus determines that a wide range of abundance values can reproduce the shape of the observed features within the error bars. Therefore, the only means to narrow the constraint is to increase the number of observed transits.

At 50 transits, the 1-5μm bandpass produces approximately a single order-of-magnitude (1.01dex) constraint at R=100 or 0.81dex at R=300. The abundance constraints produced by the 1-5μm bandpass cases at both R=50 and R=100 are comparable to those of both the 3-11μm and 3-30μm bandpasses.

4.3 Methane (CH_4)

Due to its low abundance in the modern Earth atmosphere, CH_4 is difficult to detect and ultimately determines the lower limit on the observing time required to detect all five bio-indicator molecules. Despite the larger number of transits required to detect CH_4, we can place the best constraints on its abundance due to the sensitivity of its feature strengths to small changes in abundance. In Figure 4.8, we compare the residuals of spectra generated with a $\pm$0.5dex abundance change in CH_4 and CO_2, individually. These residuals reveal that an OOM change in abundance for CH_4 result in a 3.25x greater change in the average spectral modulation, when compared to CO_2, across the entire 1-30μm bandpass.

At Earth-like abundances, CH_4 has only three discernible spectral features in the near and mid-infrared: 2.3, 3.3, and 7.6μm. The most prominent of these is centered at 7.6μm and directly overlaps with a larger N_2O feature centered at 7.7μm. Bandpass choices that exclude additional methane features will lack the ability to overcome this degeneracy. Fortunately, the 3.3μm (ν_3) feature provides an unambiguous marker for the presence of CH_4. We find that the inclusion of this feature is crucial to detecting CH_4 as neither the 5-11μm nor the 5-30μm bandpasses are capable of detecting methane within 100 transits, despite the presence of the 7.6μm (ν_4) feature. There is an additional feature at 2.3μm which, when combined with the 3.3μm band, greatly improves the detection significance.

When observing only the 3-5μm bandpass, at R=300, CH_4 is detectable with 54.9 transits and provides an abundance constraint of 1.04dex at 50 transits. Maintaining this narrow wavelength coverage and reducing to R=100, increases the necessary observation time to beyond 100 transits. However, expanding our bandpass either to the near or mid-infrared regimes proves to provide significant benefits. The near-infrared bandpass (1-5μm) requires 38.5 transits and provides a 0.63dex (at 50 transits) abundance constraint or 54.4 transits and 0.81dex for R=300 and R=100, respectively. Alternatively, observing the 3-11μm bandpass requires 34.3 transits and provides a 0.79dex (at 50 transits) abundance constraint or 61.7 transits and 0.99dex for R=300 and R=100, respectively.

Based on these results, we find that including the ν_3 feature, within the chosen bandpass, is essential to detecting and constraining CH_4. In the scenario that spectral resolution is limited to R=100, the addition of the 2.3μm feature is incredibly beneficial, providing a 0.5dex improvement in the abundance constraint and requiring only a third of the observational time. However, while it is certainly ideal to include both features if possible, it is quite noteworthy that the benefit of a higher resolution (R=300) choice, in the absence of the 2.3μm feature, outweighs the benefit of including this feature at a lower resolution (R=100).

4.4 Ozone (O_3)

Ozone is different from the other molecular species we have addressed thus far, in that its most prominent features extend further into the mid-infrared. The three primary features for O_3 are at 4.75, 9.6, and 14.2μm with the 9.6μm feature being the strongest. Conveniently, due to the location of these spectral features and our bandpass choices, we can evaluate the benefit of each additional feature, individually, on the retrieval results.

Isolating the 9.6μm feature, in the 5-11μm bandpass, requires a relatively low number of transits at only 14.9 and 18.2 transits for resolutions of R=100 and R=50, respectively. However, the abundance constraints for this bandpass exceed an order-of-magnitude at 1.41dex (R=100) and 1.58dex (R=50). If we choose to observe further into the mid-infrared (5-30μm), including the features at 9.6μm and 14.7μm, we notice only slight reductions in the required observation time and maintain larger than an order-of-magnitude constraint on both abundance values. The one noticeable benefit of including these longer wavelengths is that less than 20 transits are required to detect O_3 even at a resolution of R=30. Alternatively, extending the bandpass to 3-11μm to include the 4.75μm feature, results in a reduction of the necessary observation time to 10.5 transits for a resolution of R=100 (12.9 for R=50) and improves our abundance constraints by nearly a factor of four (0.82dex and 0.99dex) for both R=100 and R=50. It is worth noting that the 4.75μm feature has significant overlap with a minor CO_2 feature, thereby causing a degeneracy if observed without additional O_3 features. We conclude that the optimal wavelength coverage for detecting and constraining O_3 is the 3-11μm bandpass choice. Additionally, this bandpass would only require a resolution of R=50 to place an order-of-magnitude constrain on the volume mixing ratio for O_3.

4.5 Nitrous Oxide (N_2O)

Similar to O_3, the most prominent features for N_2O extend out into the longer wavelengths. N_2O's strongest spectral features are located at 4.5μm and 7.7μm, each with an adjacent smaller feature at 3.9μm and 8.6μm, respectively. Although there is a broad feature at 17μm it is overlapped by a much larger CO_2 feature.

Due to the large degree of degeneracy with the 7.6μm CH_4 feature, isolating the 7.7μm and 8.6μm features in the 5-11μm bandpass proves to be inadequate. At a

spectral resolution of R=100, the 5-11μm bandpass requires nearly twelve times as many transits ($\sim$94 transits) as the 3-11μm bandpass would require to obtain a 3.6σ detection. Extending to 30μm incorporates the 17μm feature and only reduces the observational time to 72.8 transits while the constraints still exceed 1.50dex.

We find that the 3-5μm bandpass is sufficient to detect N_2O at 14.4 transits (R=100) or 23.8 transits (R=50), making it one of the only two molecular species that can be constrained in that bandpass within relatively few transits. However, that region is too narrow to provide adequate abundance constraints, resulting in a 1.27dex constraint at 50 transits. If we expand to either the 1-5μm or the 3-11μm bandpass, our required number of transits drops to 9.2 and 7.9, respectively. The corresponding constraints at 50 transits are 0.97dex (1-5μm) and 1.02dex (3-11μm), roughly an order-of-magnitude for both. The 3-11μm region would thus allow for a 3.6σ detection in fewer transits than would be required for either O_3 or H_2O within the same regime. Likewise, the 1-5μm bandpass requires only 39.5% of the observational time, to detect N_2O, as needed to detect H_2O in the same regime. With comparable abundance constraints, the 3-11μm bandpass proves to be the optimal bandpass, requiring only 74% to 86% (R=50 to R=100) of the observation time as the 1-5μm bandpass choice.

Bandpass	Resolution	H_2O	CO_2	CH_4	O_3	N_2O
1-5μm	300	18.1	< 1	38.5	-	7.7
	100	23.3	< 1	54.4	-	9.2
	50	39.2	< 1	-	-	14.3
1-11μm	100	6.5	< 1	44	8.5	5.7
	50	7.3	< 1	52.1	9.4	7.4
1-30μm	100	6.3	< 1	43.8	8.3	5.5
	50	7.0	< 1	50	9.1	7.2
	30	8.5	1.13	-	10.9	9.0
3-5μm	300	-	1.03	54.9	-	11.2
	100	-	1.08	-	-	14.4
	50	-	1.13	-	-	23.8
3-11μm	300	11.9	< 1	34.3	8.9	5.6
	100	15.4	1.07	61.7	10.5	7.9
	50	19.6	1.11	-	12.9	10.6
3-30μm	100	14.4	< 1	60	10.2	7.7
	50	17.4	< 1	-	11.8	9.6
	30	21.1	1.15	-	14.7	12.2
5-11μm	100	33.1	-	-	14.9	94.0
	50	50	-	-	18.2	-
	30	67.2	-	-	24.3	-
5-30μm	100	22.5	6.75	-	12.9	72.8
	50	29.6	6.88	-	15.1	-
	30	36.8	6.96	-	18.2	-

Table 4.1: Shown are the number of transits required to detect each molecule to 3.6σ confidence for each of our test cases. A dash indicates that achieving a 3.6σ was not possible within 100 transits and therefore, outside the scope of this study.

Bandpass	Resolution	H_2O	CO_2	CH_4	O_3	N_2O
1-5μm	300	0.77	0.81	0.63	0.65	0.77
	100	0.99	1.01	0.81	↑	0.97
	50	1.19	1.24	1.03	↑	1.19
1-11μm	100	0.79	0.77	0.65	0.60	0.74
	50	0.99	0.93	0.81	0.75	0.92
1-30μm	100	0.77	0.74	0.63	0.59	0.72
	50	0.97	0.91	0.80	0.73	0.89
	30	1.15	1.08	0.99	0.87	1.07
3-5μm	300	↑	1.31	1.04	0.95	1.16
	100	↑	1.44	1.32	↑	1.27
	50	↑	1.86	↑	↑	1.65
3-11μm	300	0.95	0.91	0.79	0.68	0.85
	100	1.15	1.07	0.99	0.82	1.02
	50	1.37	1.29	1.30	0.99	1.23
3-30μm	100	1.10	0.74	0.94	0.79	0.99
	50	1.33	0.91	1.21	0.96	1.21
	30	1.54	1.08	1.52	1.10	1.38
5-11μm	100	1.89	-	↑	1.41	1.70
	50	2.05	-	-	1.58	2.01
	30	2.10	-	-	1.58	2.03
5-30μm	100	1.70	1.61	↑	1.23	1.50
	50	1.80	1.68	↑	1.29	1.69
	30	1.92	1.74	↑	1.33	1.78

Table 4.2: Shown are the logarithmic constraints on the vertical mixing ratios for each molecule, at 50 transits, for each of our test cases. The ↑ marker denotes an upper limit and dash represents that the parameter was entirely unconstrained by the retrieval.

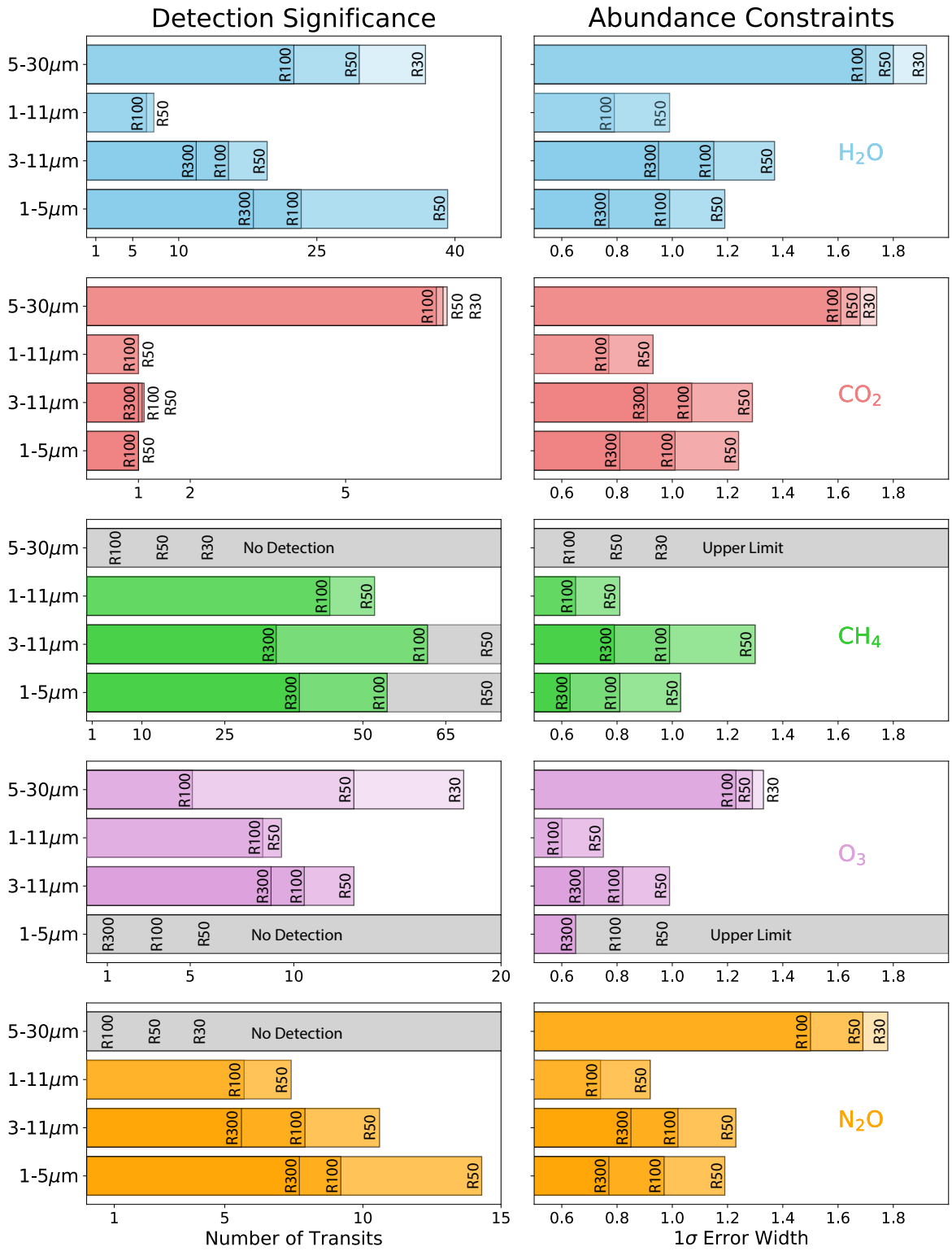

Figure 4.1: Retrieval results for each bio-indicator molecule over four bandpass choices and each spectral resolution combination. Smaller bars indicate better results: less observation time for 3.6σ detection (for the left charts) or tighter abundance constraints (for the right charts).

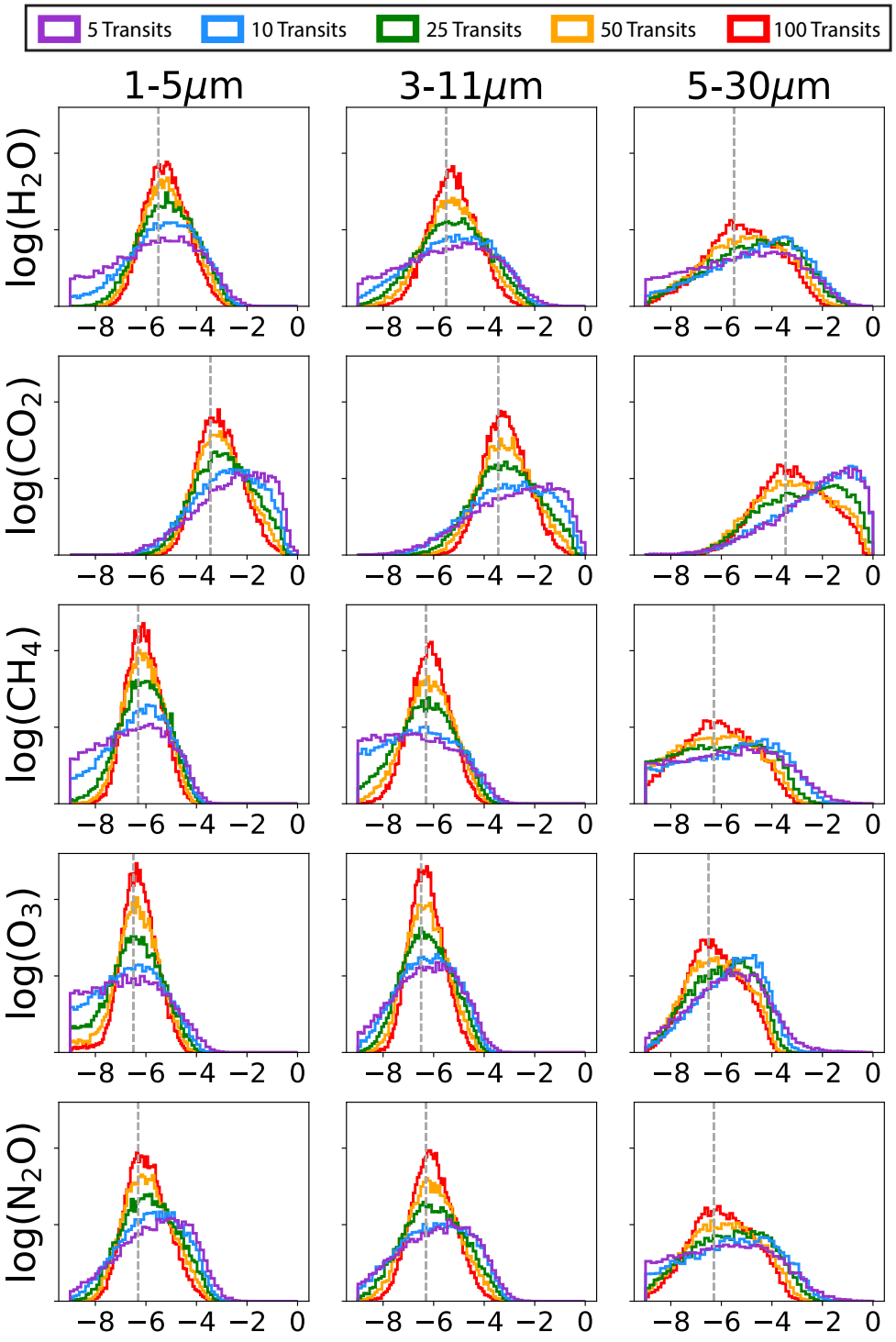

Figure 4.2: Abundance constraints for each molecule within three key bandpasses (each at R=100) as a function of the number of observed transits. The heights of each histogram window has been fixed to a constant value to allow for a direct comparison of the shape of the marginalized posterior probability distributions for each gas. The "hard edge" of some distributions, near low abundances, indicates those that extend beyond the prior range.

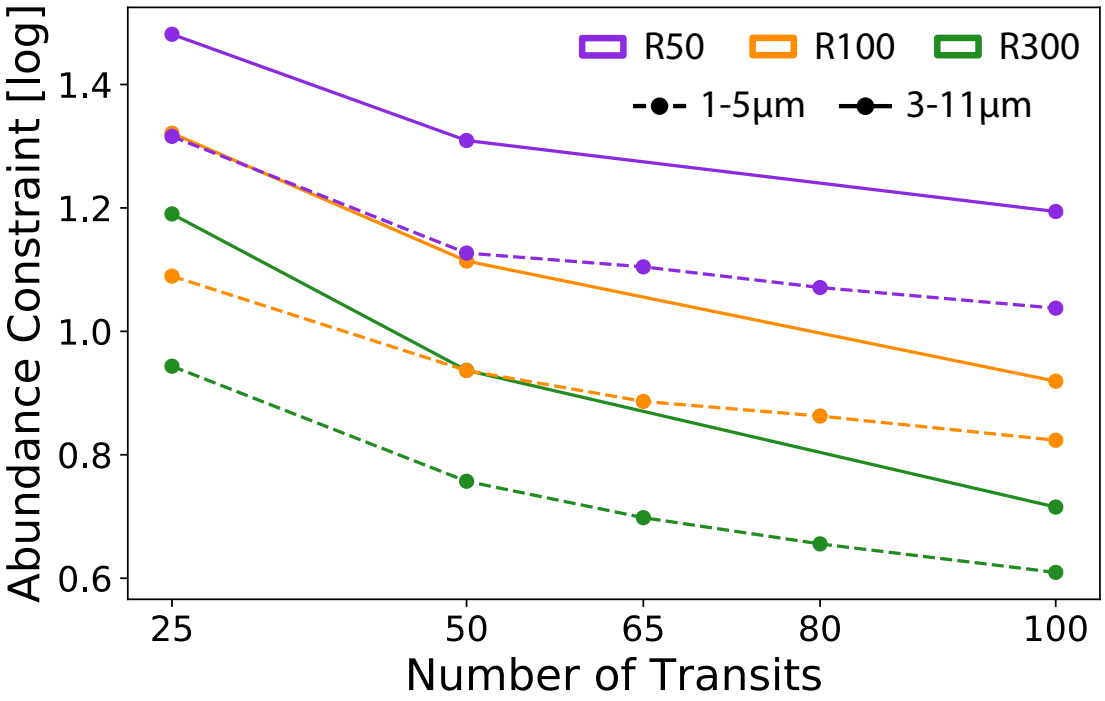

Figure 4.3: Compares the improvements of the abundance constraints for H_2O, with increasing numbers of transits at three resolutions for the two key bandpass choices.

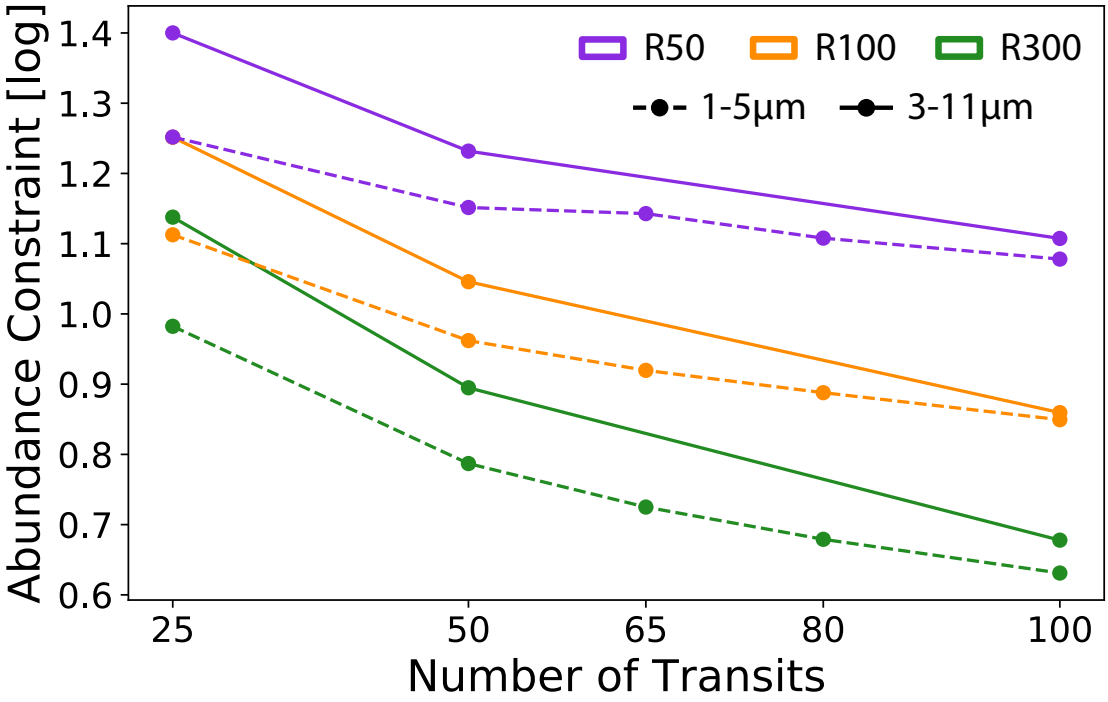

Figure 4.4: Compares the improvements of the abundance constraints for CO_2, with increasing numbers of transits at three resolutions for the two key bandpass choices.

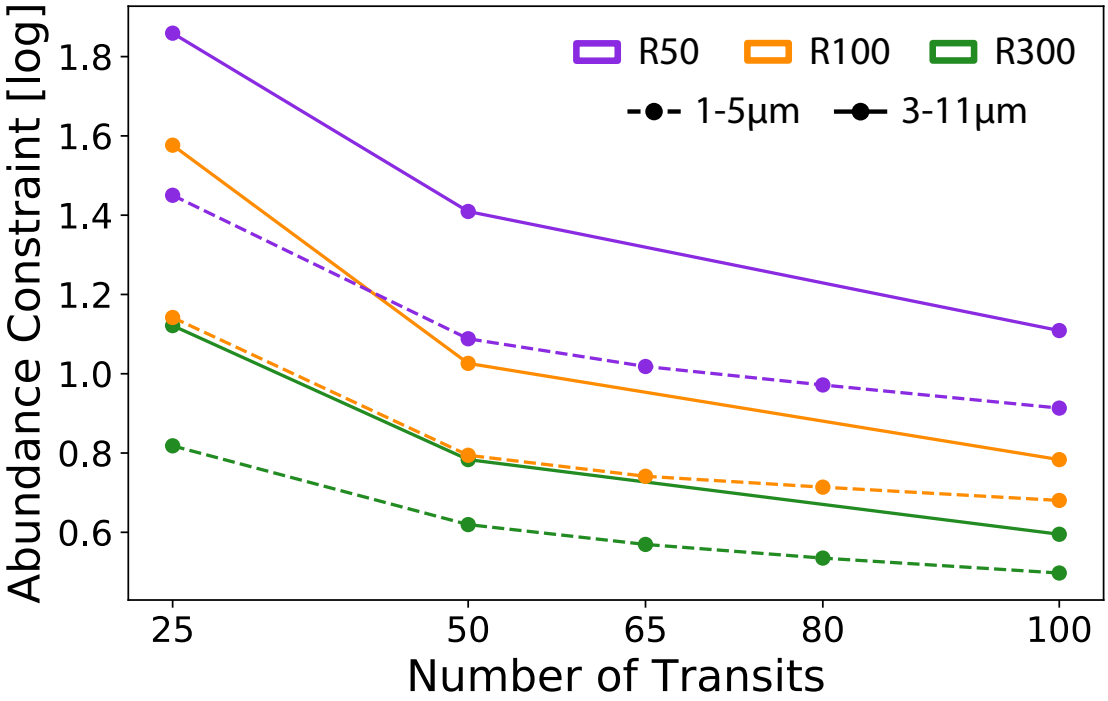

Figure 4.5: Compares the improvements of the abundance constraints for CH_4, with increasing numbers of transits at three resolutions for the two key bandpass choices.

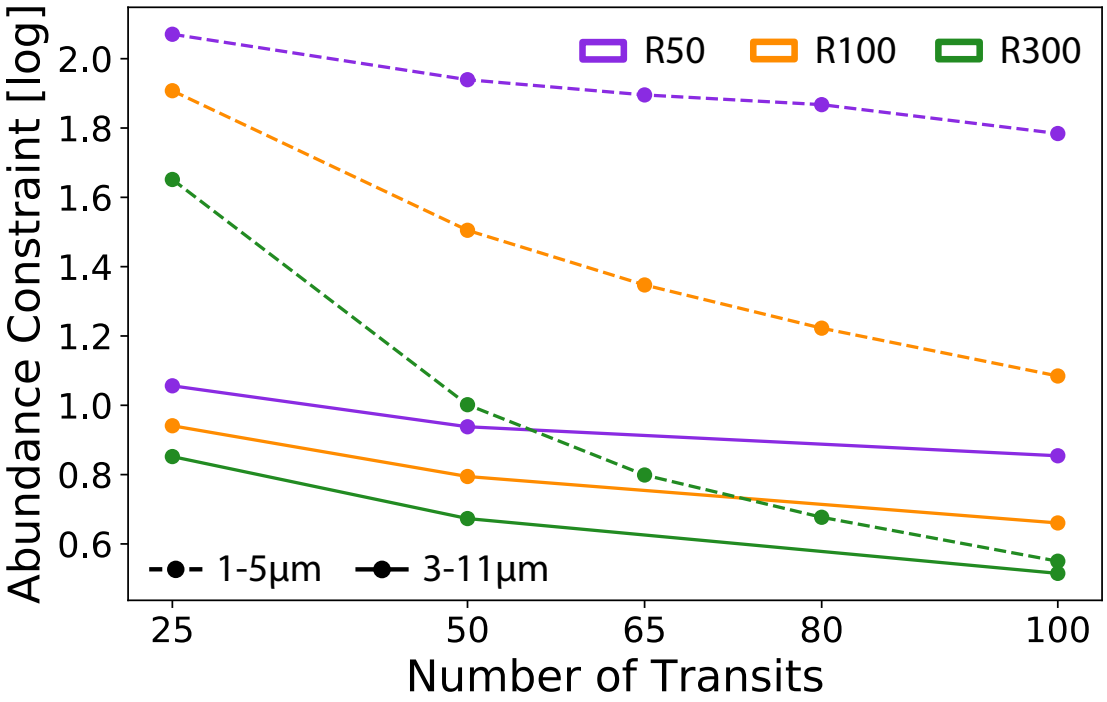

Figure 4.6: Compares the improvements of the abundance constraints for O_3, with increasing numbers of transits at three resolutions for the two key bandpass choices.

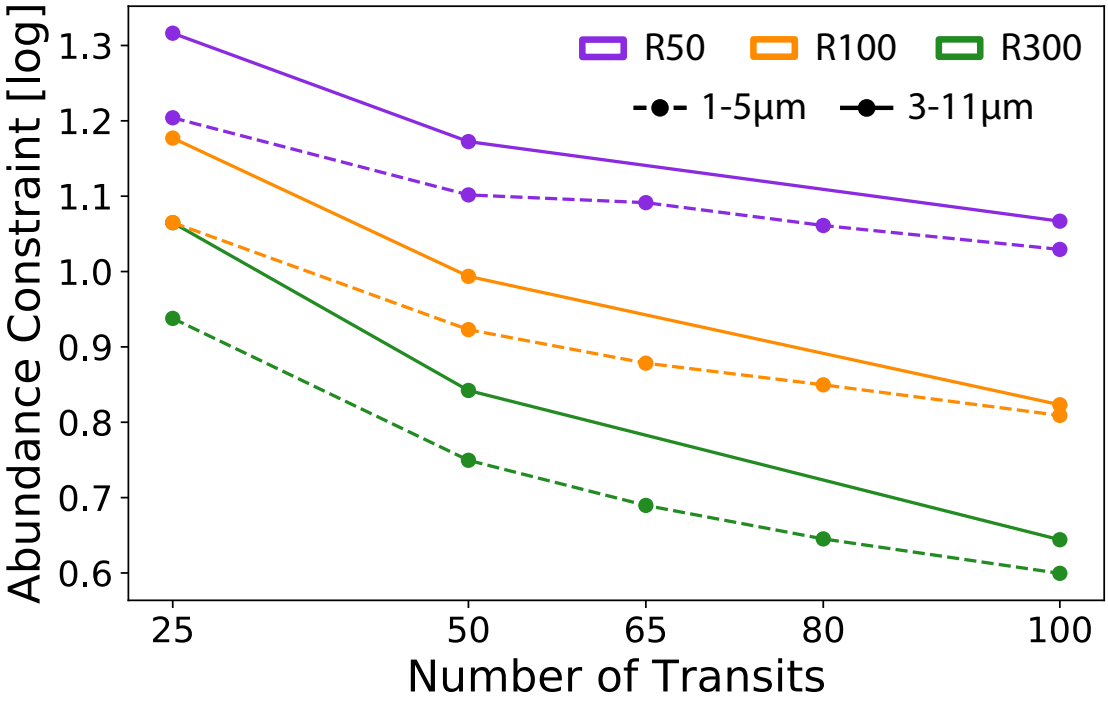

Figure 4.7: Compares the improvements of the abundance constraints for N_2O, with increasing numbers of transits at three resolutions for the two key bandpass choices.

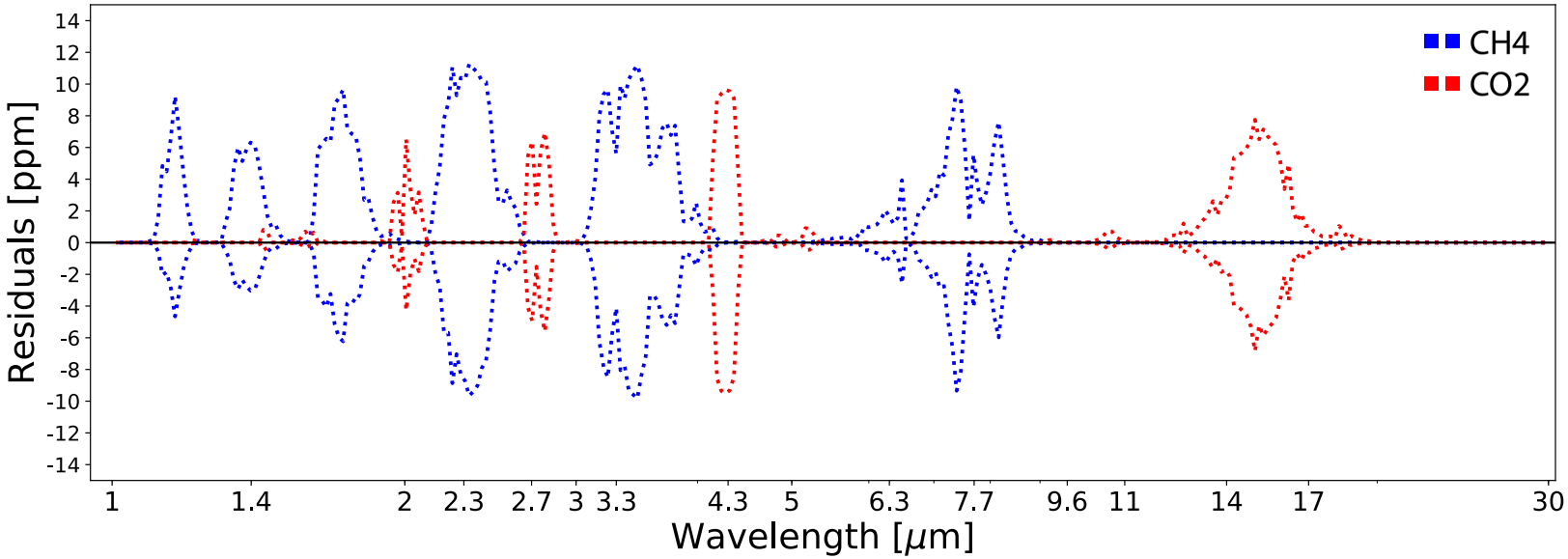

Figure 4.8: Illustrates the differences in the sensitivity of feature strengths to identical abundance changes for different molecular species. Shown, are the wavelength-dependent residuals of CO_2 (red) and CH_4 (blue) for a $\pm$0.5dex change in their abundances. The wavelengths for all key spectral features are marked on the x-axis.

Chapter 5

SUMMARY

5.1 Discussion & Conclusions

Unsurprisingly, we find that obtaining the best detection significance values and abundance constraints for all of the molecules of interest are achieved by including the broadest possible wavelength coverage at the highest possible spectral resolution. Our primary goal, however, was to determine how the detection significance and abundance constraints behave as a function of the continuous wavelength coverage and spectral resolution. In the previous section, we elaborate on the effect that additional wavelength coverage and finer resolution have on the retrieval results for each molecule individually. Below we summarize our key findings:

- When considering the contribution of additional wavelength coverage to the capability of an instrument with a continuous infrared bandpass, the most crucial spectral features (for H_2O, CO_2, CH_4, O_3, N_2O, and CO) in transmission spectra do not extend beyond 11μm.

- Utilizing a spectral resolution greater than R=100 proves to be significantly beneficial to resolving features at wavelengths shorter than 5μm. Redder wavelengths offer notably broader features, easily resolved with a resolution of R=50.

- Degeneracies caused by significantly overlapping spectral features are most easily resolved by including an additional feature for one or both molecules.

A brief summary of the crucial molecule-specific takeaways:

- When attempting to detect and constrain CH_4, the observation of the 3.3μm feature is essential. If one must opt for lower resolutions (R=100), including the 2.3μm feature is incredibly valuable. While it is certainly ideal to include both features, it is crucial to acknowledge that the benefit of a higher resolution (R=300), in the absence of the 2.3μm feature, outweighs the benefit of including this feature at a lower resolution (R=100).

- The results of this study validate an alternative to the observing strategies which are currently available for H_2O, which are limited to the weak near-infrared features. We find that the more prominent unobscured spectral feature centered at 6.3μm, combined with the dense cluster of features from other molecules at 3-5μm, provides a significant decrease in the necessary observing time to detect H_2O compared to the 1-5μm bandpass.

- CO_2, due to its very prominent features, is easily detectable even only observing the 4.3μm feature. However, increasing the wavelength coverage has statistically significant effects on the abundance constraints regardless of whether the broader bandpass includes additional CO_2 features.

- Given a $m_K = 8.0$ source star, we find that utilizing an instrument with wavelength coverage from 3-11μm, a spectral resolution of only R=50, and a 25m^2 collecting area is sufficient to detect ozone abundances representative of modern-day Earth with less than 13 transits and to constrain the abundance value within an order-of-magnitude at 50 transits.

- All of the N_2O features from 1-30μm are partially or completely degenerate with features from CO_2 or CH_4. However, under the detector set-up evaluated in this study, observing only the features in the 3-5μm regime allows for a statistically significant detection in less than 15 transits. The 1-5μm and the 3-11μm bandpasses offer comparable improvements to both the detection significance and abundance constraints.

The ability to detect and constrain the five biologically relevant molecular species in the atmosphere of an Earth-analog should be the benchmark by which the next-generation of exoplanet observatories are designed. The detection of significant amounts of CH_4 in tandem with O_3 and/or N_2O would constitute a promising indicator of biogenic origins. However, as it has been laboriously stated, CH_4 is the most challenging molecule to detect in this study and will prove to be the limiting variable in the development of a detector for these purposes. Unlike the other molecules considered here, CH_4 does not possess broad unobscured features in the mid-infrared and therefore does not have the advantage of relaxed spectral resolution requirements. It is important to acknowledge, however; that this is not an argument against observing mid-infrared wavelengths, which have been shown to be immensely valuable in the detection and constraint of all of the other molecular species in this study. Rather, our intention is to highlight that the choice of wavelength coverage for a next-generation near-to-mid-infrared spectrometer, particularly on the blue end of the bandpass, must be influenced by one or both of the near-infrared CH_4 features. We conclude that a near-to-mid-infrared spectrometer, aboard a next-generation space-based telescope (with a collecting area of 25m^2), boasting a bandpass including features between $\sim$2-11μm and a resolution of R$\simeq$50-300 would prove capable of detecting and constraining all of the key bio-indicator gasses in Earth's atmosphere. While the 2-11μm bandpass was not explicitly probed in this study, our retrieval results indicate that it would

provide 3.6σ detections in less transits and narrower abundance constraints than either the 1-5μm or 3-11μm bandpasses studies here. Figure 4.1 provides a side-by-side comparison of the retrieval results of these bandpasses.

5.2 Implications for Next-Generation Observatories

Our work has been motivated by the desire within the exoplanet community to characterize the atmospheres of temperate terrestrial planets beyond our Solar System. The detection of molecular biosignatures on these small rocky planets looms just beyond the capabilities of current space-based telescopes. A future facility with broad continuous wavelength coverage in the near and mid-infrared combined with detectors capable of driving observational noise down to the astrophysical noise floor will have what it takes to comprehensively probe the climate and composition of terrestrial exoplanet atmospheres.

The 2020 Decadal Survey will consider four flagship mission concepts including one of particular interest to this study, the Origins Space Telescope. The Origins concept includes a near-to-mid-infrared spectrograph boasting an impressive 2.8-20μm continuous bandpass ranging from R$\simeq$50-300 with detectors designed to reduce instrument noise to approximately 5ppm (OST-STDT[1]). Although it excludes the 2.3μm feature for CH_4, the design of this instrument strongly aligns with the findings in this work for the optimal observational setup for both detecting the presence and constraining the abundances of Earth-like biosignatures.

We look to expand upon this work by testing a subset of this analysis to a broader range of atmospheric compositions in order to determine the possibility of distinguishing several plausible atmospheric compositions on known terrestrial planets and those soon-to-be-discovered by *TESS* (Barclay et al. 2017). Additionally, we acknowledge

[1]https://asd.gsfc.nasa.gov/firs/docs/OriginsVolume1MissionConceptStudyReport.pdf

the benefit of thermal emission spectroscopy for characterizing the thermal structure of exoplanetary atmospheres and providing additional information on the molecular abundances. Therefore, we aim to explore the effect of these observational parameters on a similar grid of synthetic thermal emission spectra. To this end, we anticipate that the synthesis of transmission and thermal emission as well as reflected light spectroscopy to be essential to the comprehensive understanding of these exoplanetary environments.

Chapter 6

ORIGINS SPACE TELESCOPE

6.1 Overview of Mission Concept & Goals

The Origins Space Telescope (*Origins*) Mission Concept was generated in response to the call for large mission concepts to serve as NASA's flagship observatory of the 2030s, immediately following *JWST*. The primary science objectives of *Origins* seek to answer three questions:

- How do galaxies form stars, make metals, and grow their central supermassive black holes from reionization to today?
- How do the conditions for habitability develop during the process of planet formation?
- Do planets orbiting M-dwarf stars support life?

To answer this third question, the *Origins* Concept seeks to build upon the heritage of missions like *Hubble*, *Spitzer*, and *JWST* as it further refines the technique of transit spectroscopy. *Origins* would utilize active cryo-cooling and next-generation detectors (described in Section 2.3) in order to push observational noise down to the astrophysical noise limit. The on-board instrument of primary interest to our study is the Mid-Infrared Spectrometer Camera Transit Spectrometer or MISC-T instrument. This proposed instrument would boast broad continuous mid-infrared wavelength coverage, without the use of multiple observing modes, combined with moderate spectral resolutions across the entire bandpass.

The goal of this instrument, in seeking to answer the third question stated above, is to detect the presence and constrain the abundances of molecular biosignatures in the atmospheres of temperate terrestrial exoplanets.

6.2 Contributions to Exoplanets Working Group

The MISC-T instrument would be primarily used to address the questions of habitability for terrestrial-sized planets found orbiting M-dwarf stars. Therefore, the *Origins* Exoplanets Working Group was assembled with the intent of studying the technology requirements for the MISC-T instrument in order for it to plausibly achieve this goal, were it to be launched. As members of the Working Group, we performed hundreds of atmospheric retrievals on synthetic spectra of an Earth-like composition atmosphere scaled onto TRAPPIST-1e with the host star at various magnitudes. The primary collecting area of the proposed *Origins* mirror would be approximately 25m^2. Our grid of spectra was therefore produced over a range of wavelength coverages, spectral resolutions, and signal-to-noise (realized as the number of observed transits). Prior to our involvement, the Concept A or nominal design for the MISC-T instrument included a bandpass from 5-30μm with a tentative resolution of R=100. Our study explored wavelength coverage cutoffs specifically related to the detector capabilities being studying by a separate detector engineering team. Furthermore, we explored spectral resolution values from R=30 to 300 to determine the trade space between various wavelength coverages and resolution values. The set-up for this retrieval study was identical to the one described in Section 2 with the exception being that different wavelength ranges were explored and retrievals were performed for both transmission and thermal emission spectra.

The conclusions of our analysis informed the design specifications of the MISC-T instrument by extending the blue wavelength cutoff from 5μm to 2.8μm to include the

dense cluster of spectral features between 4-5μm and most importantly, the 3.3μm CH_4 feature. Additionally, our results emphasized the previously underestimated benefit of increased spectral resolution below 5μm. Through our retrieval analysis, we were further able to refine the red end of the wavelength coverage to 20μm, noting that the inclusion of bands between 10.5-20μm in thermal emission greatly narrowed our constraints of the planet's surface temperature. Likewise, features beyond 10.5μm in transmission and beyond 20μm in emission did little to narrow parameter constraints or improve molecular detection significance values. Figures 6.1 through 6.4 illustrate these findings and were produced by the IPAC graphics team for the Origins Mission Concept Study Report utilizing the data from our retrieval study.

The details, specifications, and figures included throughout this chapter were sourced from the aforementioned Origins Mission Concept Study Report (2019).

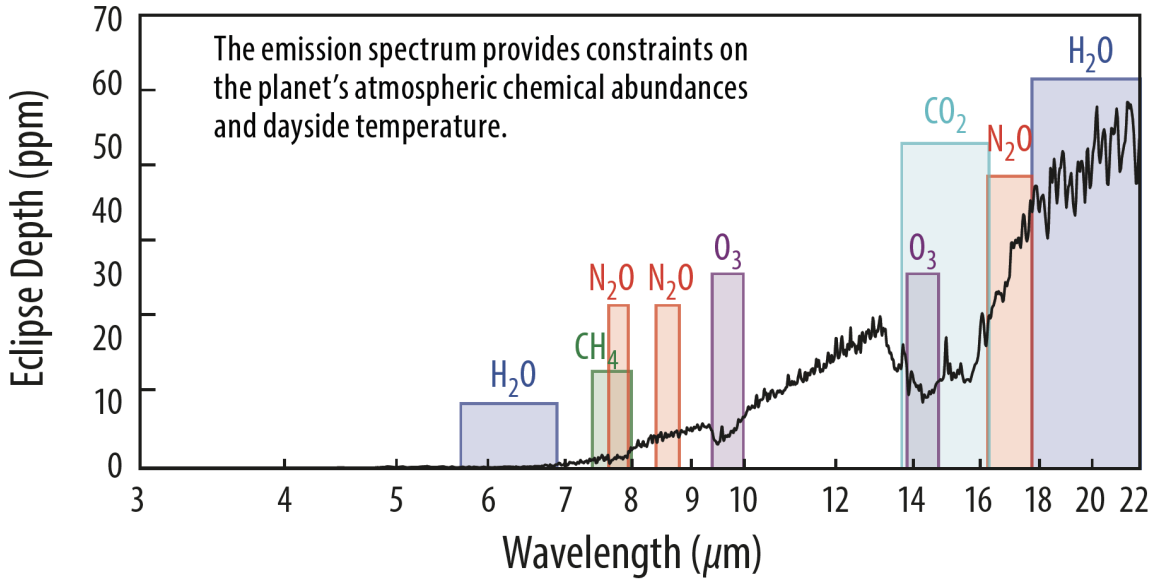

Figure 6.1: Synthetic thermal emission spectra generating using identical forward model parameters as included in Table 2.1. Additional parameters were included for the thermal emission spectra to define a temperature-pressure profile not constant with altitude (like in the transmission forwards model) as emission spectra probe physical characteristics deeper in the planet's atmosphere. The thermal emission spectra is reproduced here to illustrate the spectral features present across the wavelength coverage explored in our *Origins* Concept study.

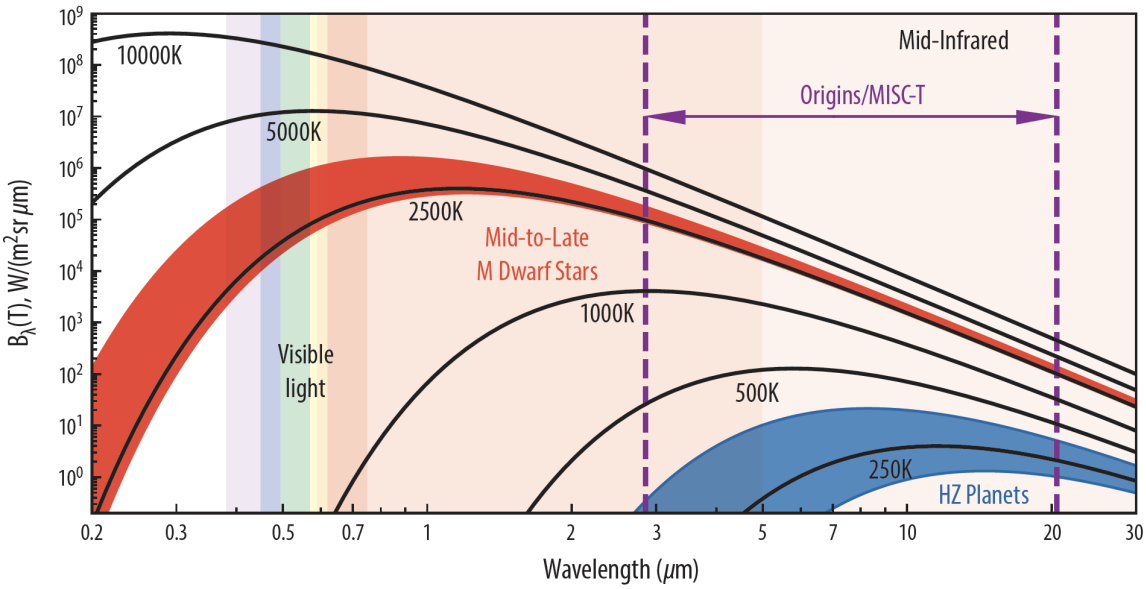

Figure 6.2: Blackbody (BB) irradiance of objects over a range of temperatures (250-10,000K). The red contour illustrates the range of BB spectra for the temperatures of M-dwarf stars, while the blue contour represents the range of BB spectra for temperate (habitable-zone) planets. The bandpass of the MISC-T instrument would cover the near-to-mid-infrared wavelengths ideally suited to study the thermal emission spectra of temperate planets given that the planet/star flux ratio is maximized in this regime.

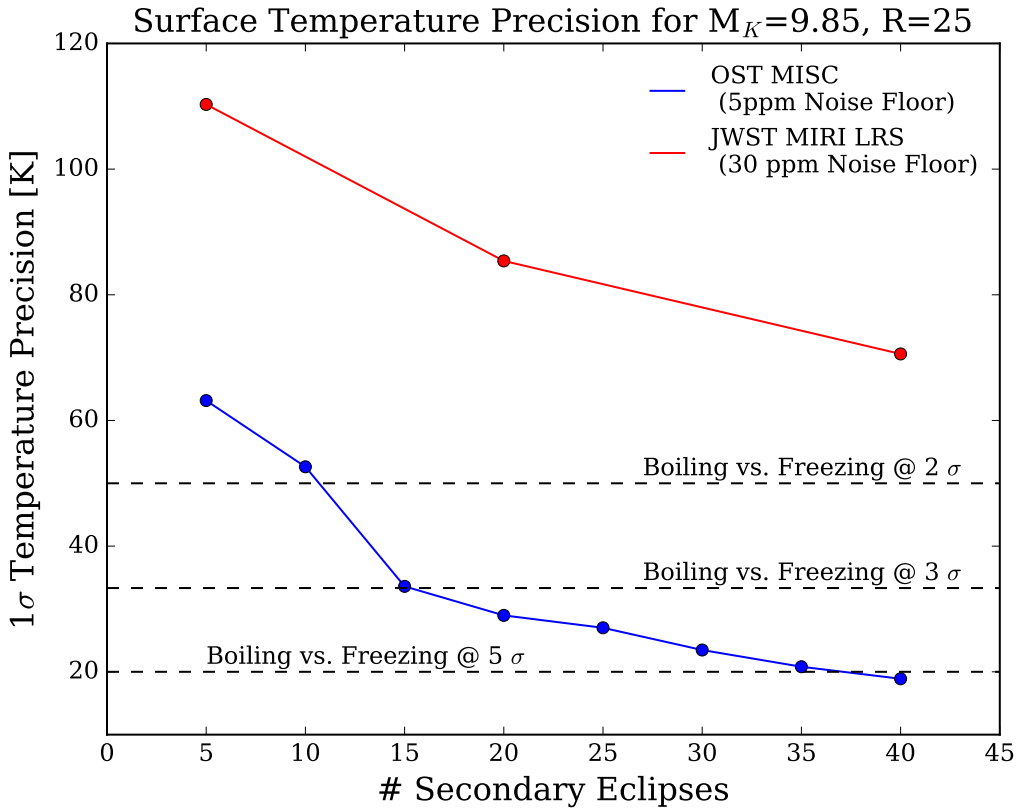

Figure 6.3: Posteriors for the Surface Temperature parameter evaluated over increasing observed secondary eclipses. The dashed lines indicate 2σ, 3σ, and 5σ confidence levels, respectively.

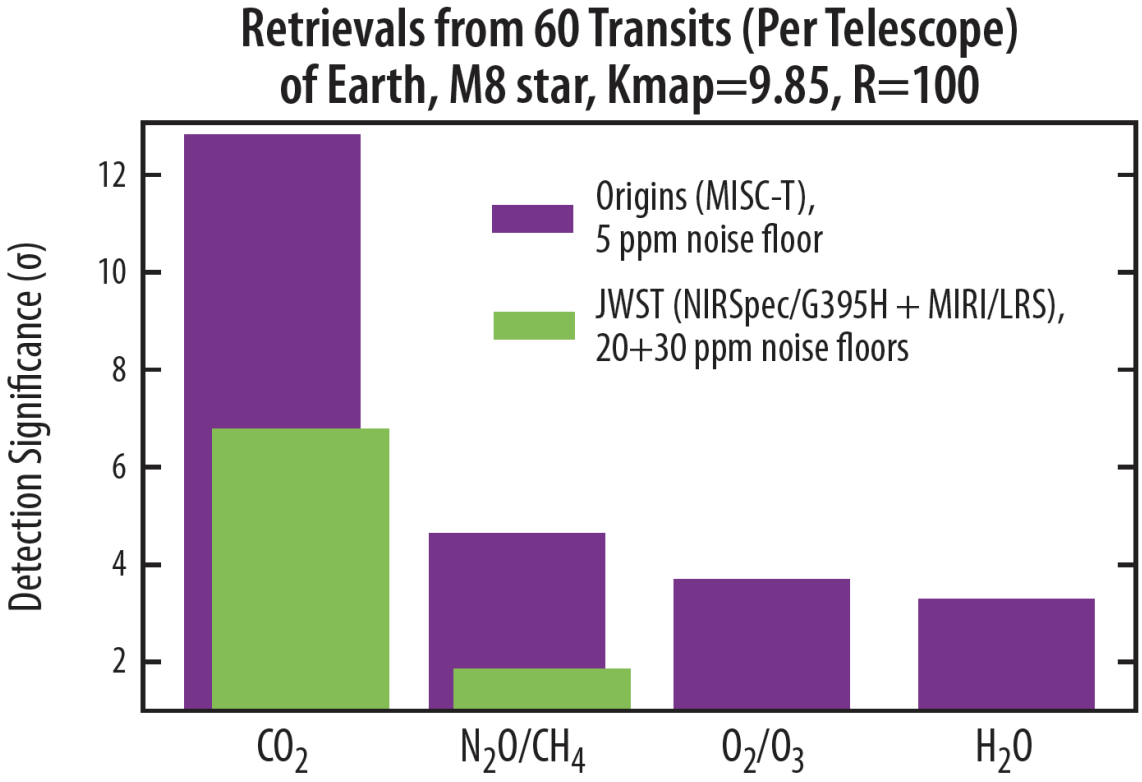

Figure 6.4: Detection significance values displayed as σ confidence levels when retrieving for each molecular species (or combination of molecules i.e. N_2O+CH_4) in transmission spectra. The values for O_2/O_3 indicate the result for O_3 (for Origins) and the combined features of O_2 and O_3 (for JWST). Different from the study described in Chapters 2-5, the transmission spectra produced for this retrieval analysis was generated using a host star with a mag_K=9.85 to represent the mean magnitude of the 18 brightest targets in the estimates TESS yield (Barclay et al. 2018).

REFERENCES

Barclay, T., J. Pepper and E. V. Quintana, "A Revised Exoplanet Yield from the Transiting Exoplanet Survey Satellite (TESS)", **239**, 1, 2 (2018).

Barstow, J. K., S. Aigrain, P. G. J. Irwin, T. Hackler, L. N. Fletcher, J. M. Lee and N. P. Gibson, "Clouds on the Hot Jupiter HD189733b: Constraints from the Reflection Spectrum", **786**, 2, 154 (2014).

Barstow, J. K. and P. G. J. Irwin, "Habitable worlds with JWST: transit spectroscopy of the TRAPPIST-1 system?", **461**, 1, L92–L96 (2016).

Batalha, N. E., N. K. Lewis, M. R. Line, J. Valenti and K. Stevenson, "Strategies for Constraining the Atmospheres of Temperate Terrestrial Planets with JWST", **856**, 2, L34 (2018).

Batalha, N. E. and M. R. Line, "Information Content Analysis for Selection of Optimal JWST Observing Modes for Transiting Exoplanet Atmospheres", **153**, 4, 151 (2017).

Beichman, C., B. Benneke, H. Knutson, R. Smith, P.-O. Lagage, C. Dressing, D. Latham, J. Lunine, S. Birkmann, P. Ferruit, G. Giardino, E. Kempton, S. Carey, J. Krick, P. D. Deroo, A. Mand ell, M. E. Ressler, A. Shporer, M. Swain, G. Vasisht, G. Ricker, J. Bouwman, I. Crossfield, T. Greene, S. Howell, J. Christiansen, D. Ciardi, M. Clampin, M. Greenhouse, A. Sozzetti, P. Goudfrooij, D. Hines, T. Keyes, J. Lee, P. McCullough, M. Robberto, J. Stansberry, J. Valenti, M. Rieke, G. Rieke, J. Fortney, J. Bean, L. Kreidberg, D. Ehrenreich, D. Deming, L. Albert, R. Doyon and D. Sing, "Observations of Transiting Exoplanets with the James Webb Space Telescope (JWST)", **126**, 946, 1134 (2014).

Benneke, B. and S. Seager, "How to Distinguish between Cloudy Mini-Neptunes and Water/Volatile-dominated Super-Earths", **778**, 2, 153 (2013).

Buchner, J., A. Georgakakis, K. Nandra, L. Hsu, C. Rangel, M. Brightman, A. Merloni, M. Salvato, J. Donley and D. Kocevski, "X-ray spectral modelling of the AGN obscuring region in the CDFS: Bayesian model selection and catalogue", **564**, A125 (2014).

Catling, D. and J. Kasting, *Planetary Atmospheres and Life*, pp. 91 – 116 (Cambridge University Press, United Kingdom, 2007).

Chapman, J. W., R. T. Zellem, M. R. Line, G. Vasisht, G. Bryden, K. Willacy, A. R. Iyer, J. Bean, N. B. Cowan, J. J. Fortney, C. A. Griffith, T. Kataria, E. M. R. Kempton, L. Kreidberg, J. I. Moses, K. B. Stevenson and M. R. Swain, "Quantifying the Impact of Spectral Coverage on the Retrieval of Molecular Abundances from Exoplanet Transmission Spectra", **129**, 980, 104402 (2017).

Cockell, C. S., L. Kaltenegger and J. A. Raven, "Cryptic Photosynthesis-Extrasolar Planetary Oxygen Without a Surface Biological Signature", Astrobiology **9**, 7, 623–636 (2009).

Cowan, N. B., T. Greene, D. Angerhausen, N. E. Batalha, M. Clampin, K. Colón, I. J. M. Crossfield, J. J. Fortney, B. S. Gaudi, J. Harrington, N. Iro, C. F. Lillie, J. L. Linsky, M. Lopez-Morales, A. M. Mandell and K. B. Stevenson, "Characterizing Transiting Planet Atmospheres through 2025", **127**, 949, 311 (2015).

Deming, D., S. Seager, J. Winn, E. Miller-Ricci, M. Clampin, D. Lindler, T. Greene, D. Charbonneau, G. Laughlin, G. Ricker, D. Latham and K. Ennico, "Discovery and Characterization of Transiting Super Earths Using an All-Sky Transit Survey and Follow-up by the James Webb Space Telescope", **121**, 883, 952 (2009).

Domagal-Goldman, S. D., A. Segura, M. W. Claire, T. D. Robinson and V. S. Meadows, "Abiotic Ozone and Oxygen in Atmospheres Similar to Prebiotic Earth", **792**, 2, 90 (2014).

Gillon, M., E. Jehin, S. M. Lederer, L. Delrez, J. de Wit, A. Burdanov, V. Van Grootel, A. J. Burgasser, A. H. M. J. Triaud, C. Opitom, B.-O. Demory, D. K. Sahu, D. Bardalez Gagliuffi, P. Magain and D. Queloz, "Temperate Earth-sized planets transiting a nearby ultracool dwarf star", **533**, 7602, 221–224 (2016).

Gillon, M., A. H. M. J. Triaud, B.-O. Demory, E. Jehin, E. Agol, K. M. Deck, S. M. Lederer, J. de Wit, A. Burdanov, J. G. Ingalls, E. Bolmont, J. Leconte, S. N. Raymond, F. Selsis, M. Turbet, K. Barkaoui, A. Burgasser, M. R. Burleigh, S. J. Carey, A. Chaushev, C. M. Copperwheat, L. Delrez, C. S. Fernand es, D. L. Holdsworth, E. J. Kotze, V. Van Grootel, Y. Almleaky, Z. Benkhaldoun, P. Magain and D. Queloz, "Seven temperate terrestrial planets around the nearby ultracool dwarf star TRAPPIST-1", **542**, 7642, 456–460 (2017).

Glass, J. D. and W. D. Blair, "Detection of rayleigh targets using adjacent matched filter samples", IEEE Transactions on Aerospace Electronic Systems **51**, 3, 1927–1941 (2015).

Glass, J. D., W. D. Blair and A. D. Lanterman, "Joint-Bin Monopulse Processing of Rayleigh Targets", IEEE Transactions on Signal Processing **63**, 24, 6673–6683 (2015).

Gordon, I., L. Rothman, C. Hill, R. Kochanov, Y. Tan, P. Bernath, M. Birk, V. Boudon, A. Campargue, K. Chance, B. Drouin, J.-M. Flaud, R. Gamache, J. Hodges, D. Jacquemart, V. Perevalov, A. Perrin, K. Shine, M.-A. Smith, J. Tennyson, G. Toon, H. Tran, V. Tyuterev, A. Barbe, A. Császár, V. Devi, T. Furtenbacher, J. Harrison, J.-M. Hartmann, A. Jolly, T. Johnson, T. Karman, I. Kleiner, A. Kyuberis, J. Loos, O. Lyulin, S. Massie, S. Mikhailenko, N. Moazzen-Ahmadi, H. Müller, O. Naumenko, A. Nikitin, O. Polyansky, M. Rey, M. Rotger, S. Sharpe, K. Sung, E. Starikova, S. Tashkun, J. V. Auwera, G. Wagner, J. Wilzewski, P. Wcisło, S. Yu and E. Zak, "The hitran2016 molecular spectroscopic database", Journal of Quantitative Spectroscopy and Radiative Transfer **203**, 3 – 69 (2017).

Greene, T. P., M. R. Line, C. Montero, J. J. Fortney, J. Lustig-Yaeger and K. Luther, "Characterizing Transiting Exoplanet Atmospheres with JWST", **817**, 1, 17 (2016).

Grimm, S. L., B.-O. Demory, M. Gillon, C. Dorn, E. Agol, A. Burdanov, L. Delrez, M. Sestovic, A. H. M. J. Triaud, M. Turbet, É. Bolmont, A. Caldas, J. de Wit, E. Jehin, J. Leconte, S. N. Raymond, V. Van Grootel, A. J. Burgasser, S. Carey, D. Fabrycky, K. Heng, D. M. Hernandez, J. G. Ingalls, S. Lederer, F. Selsis and D. Queloz, "The nature of the TRAPPIST-1 exoplanets", **613**, A68 (2018).

Hardegree-Ullman, K. K., M. C. Cushing, P. S. Muirhead and J. L. Christiansen, "Kepler Planet Occurrence Rates for Mid-type M Dwarfs as a Function of Spectral Type", **158**, 2, 75 (2019).

Harman, C. E., R. Felton, R. Hu, S. D. Domagal-Goldman, A. Segura, F. Tian and J. F. Kasting, "Abiotic O_2 Levels on Planets around F, G, K, and M Stars: Effects of Lightning-produced Catalysts in Eliminating Oxygen False Positives", **866**, 1, 56 (2018).

Harman, C. E., E. W. Schwieterman, J. C. Schottelkotte and J. F. Kasting, "Abiotic O_2 Levels on Planets around F, G, K, and M Stars: Possible False Positives for Life?", **812**, 2, 137 (2015).

Kasting, J. F., "Methane and climate during the Precambrian Era", Geochimica et Cosmochimica Acta Supplement **73**, A625 (2009).

Kempton, E. M. R., J. L. Bean, D. R. Louie, D. Deming, D. D. B. Koll, M. Mansfield, J. L. Christiansen, M. López-Morales, M. R. Swain, R. T. Zellem, S. Ballard, T. Barclay, J. K. Barstow, N. E. Batalha, T. G. Beatty, Z. Berta-Thompson, J. Birkby, L. A. Buchhave, D. Charbonneau, N. B. Cowan, I. Crossfield, M. de Val-Borro, R. Doyon, D. Dragomir, E. Gaidos, K. Heng, R. Hu, S. R. Kane, L. Kreidberg, M. Mallonn, C. V. Morley, N. Narita, V. Nascimbeni, E. Pallé, E. V. Quintana, E. Rauscher, S. Seager, E. L. Shkolnik, D. K. Sing, A. Sozzetti, K. G. Stassun, J. A. Valenti and C. von Essen, "A Framework for Prioritizing the TESS Planetary Candidates Most Amenable to Atmospheric Characterization", **130**, 993, 114401 (2018).

Kochanov, R., I. Gordon, L. Rothman, P. Wcisło, C. Hill and J. Wilzewski, "Hitran application programming interface (hapi): A comprehensive approach to working with spectroscopic data", Journal of Quantitative Spectroscopy and Radiative Transfer **177**, 15 – 30, xVIIIth Symposium on High Resolution Molecular Spectroscopy (HighRus-2015), Tomsk, Russia (2016).

Krissansen-Totton, J., D. S. Bergsman and D. C. Catling, "On Detecting Biospheres from Chemical Thermodynamic Disequilibrium in Planetary Atmospheres", Astrobiology **16**, 1, 39–67 (2016).

Krissansen-Totton, J., R. Garland, P. Irwin and D. C. Catling, "Detectability of Biosignatures in Anoxic Atmospheres with the James Webb Space Telescope: A TRAPPIST-1e Case Study", **156**, 3, 114 (2018).

Léger, A., "Strategies for Remote Detection of Life - DARWIN-IRSI and TPF missions -", Advances in Space Research **25**, 11, 2209–2223 (2000).

Léger, A., M. Pirre and F. J. Marceau, "Search for primitive life on a distant planet: relevance of 02 and 03 detections", **277**, 309 (1993).

Line, M. R. and V. Parmentier, "The Influence of Nonuniform Cloud Cover on Transit Transmission Spectra", **820**, 1, 78 (2016).

Line, M. R., A. S. Wolf, X. Zhang, H. Knutson, J. A. Kammer, E. Ellison, P. Deroo, D. Crisp and Y. L. Yung, "A Systematic Retrieval Analysis of Secondary Eclipse Spectra. I. A Comparison of Atmospheric Retrieval Techniques", **775**, 2, 137 (2013).

Lustig-Yaeger, J., V. S. Meadows and A. P. Lincowski, "The Detectability and Characterization of the TRAPPIST-1 Exoplanet Atmospheres with JWST", **158**, 1, 27 (2019).

Matsuo, T., T. Greene, T. L. Roellig, R. E. McMurray, R. R. Johnson, A. Kashani, S. Goda, M. Ido, S. Ito, T. Tsuboi, T. Yamamuro, Y. Ikeda, H. Shibai, T. Sumi, I. Sakon and K. Ennico-Smith, "A highly stable spectrophotometric capability for the Origins Space Telescope (OST) mid-infrared imager, spectrometer, coronagraph (MISC)", in "Space Telescopes and Instrumentation 2018: Optical, Infrared, and Millimeter Wave", vol. 10698, pp. 1218 – 1229, International Society for Optics and Photonics (SPIE, 2018).

Meadows, V. S., "Reflections on O_2 as a Biosignature in Exoplanetary Atmospheres", Astrobiology **17**, 10, 1022–1052 (2017).

Meadows, V. S., C. T. Reinhard, G. N. Arney, M. N. Parenteau, E. W. Schwieterman, S. D. Domagal-Goldman, A. P. Lincowski, K. R. Stapelfeldt, H. Rauer, S. DasSarma, S. Hegde, N. Narita, R. Deitrick, J. Lustig-Yaeger, T. W. Lyons, N. Siegler and J. L. Grenfell, "Exoplanet Biosignatures: Understanding Oxygen as a Biosignature in the Context of Its Environment", Astrobiology **18**, 6, 630–662 (2018).

Morley, C. V., L. Kreidberg, Z. Rustamkulov, T. Robinson and J. J. Fortney, "Observing the Atmospheres of Known Temperate Earth-sized Planets with JWST", **850**, 2, 121 (2017).

Quirrenbach, A., P. J. Amado, I. Ribas, A. Reiners, J. A. Caballero, W. Seifert, J. Aceituno, M. Azzaro, D. Baroch, D. Barrado, F. Bauer, S. Becerril, V. J. S. Bèjar, D. Benítez, M. Brinkmöller, C. Cardona Guillén, C. Cifuentes, J. Colomé, M. Cortés-Contreras, S. Czesla, S. Dreizler, K. Frölich, B. Fuhrmeister, D. Galadí-Enríquez, J. I. González Hernández, R. González Peinado, E. W. Guenther, E. de Guindos, H. J. Hagen, A. P. Hatzes, P. H. Hauschildt, J. Helmling, T. Henning, O. Herbort, L. Hernández Castaño, E. Herrero, D. Hintz, S. V. Jeffers, E. N. Johnson, E. de Juan, A. Kaminski, H. Klahr, M. Kürster, M. Lafarga, L. Sairam, M. Lampón, L. M. Lara, R. Launhardt, M. López del Fresno, M. López-Puertas, R. Luque, H. Mandel, E. G. Marfil, E. L. Martín, S. Martín-Ruiz, R. J. Mathar, D. Montes, J. C. Morales, E. Nagel, L. Nortmann, G. Nowak, E. Pallé, V. M. Passegger, A. Pavlov, S. Pedraz, D. Pérez-Medialdea, M. Perger, R. Rebolo, S. Reffert, E. Rodríguez, C. Rodríguez López, A. Rosich, S. Sabotta, S. Sadegi, M. Salz, A. Sánchez-López, J. Sanz-Forcada, P. Sarkis, S. Schäfer, J. Schiller,

J. H. M. M. Schmitt, P. Schöfer, A. Schweitzer, D. Shulyak, E. Solano, O. Stahl, M. Tala Pinto, T. Trifonov, M. R. Zapatero Osorio, F. Yan, M. Zechmeister, F. J. Abellán, M. Abril, F. J. Alonso-Floriano, M. Ammler-von Eiff, G. Angladа-Escudé, H. Anwand-Heerwart, B. Arroyo-Torres, Z. M. Berdiñas, G. Bergondy, M. Blümcke, C. del Burgo, J. Cano, J. Carro, M. C. Cárdenas, E. Casal, A. Claret, E. Díez-Alonso, M. Doellinger, R. Dorda, C. Feiz, M. Fernández, I. M. Ferro, G. Gaisné, I. Gallardo, M. C. Gálvez-Ortiz, A. García-Piquer, M. L. García-Vargas, R. Garrido, L. Gesa, V. Gómez Galera, E. González-Álvarez, L. González-Cuesta, S. Grohnert, U. Grözinger, J. Guàrdia, A. Guijarro, R. P. Hedrosa, D. Hermann, I. Hermelo, R. Hernández Arabí, F. Hernández Hernando, D. Hidalgo, G. Holgado, A. Huber, K. Huber, P. Huke, M. Kehr, M. Kim, R. Klein, J. Klüter, A. Klutsch, F. Labarga, N. Labiche, A. Lamert, W. Laun, F. J. Lázaro, U. Lemke, R. Lenzen, M. Llamas, J. L. Lizon, N. Lodieu, M. J. López González, M. López-Morales, J. F. López Salas, J. López-Santiago, H. Magán Madinabeitia, U. Mall, L. Mancini, J. A. Marín Molina, H. Martínez-Rodríguez, D. Maroto Fernández, C. J. Marvin, E. Mirabet, M. E. Moreno-Raya, A. Moya, R. Mundt, V. Naranjo, J. Panduro, J. Pascual, A. Pérez-Calpena, M. A. C. Perryman, M. Pluto, A. Ramón, P. Redondo, S. Reinhart, P. Rhode, H. W. Rix, F. Rodler, R. R. Rohloff, E. Sánchez-Blanco, M. A. Sánchez Carrasco, L. F. Sarmiento, C. Schmidt, C. Storz, J. B. P. Strachan, J. Stürmer, J. C. Suárez, H. M. Tabernero, L. Tal-Or, S. M. Tulloch, R. G. Ulbrich, G. Veredas, J. L. Vico Linares, M. Vidal-Dasilva, F. Vilardell, K. Wagner, J. Winkler, V. Wolthoff, W. Xu and Z. Zhao, "CARMENES: high-resolution spectra and precise radial velocities in the red and infrared", vol. 10702 of *Society of Photo-Optical Instrumentation Engineers (SPIE) Conference Series*, p. 107020W (2018).

Robinson, T. D., J. J. Fortney and W. B. Hubbard, "Analytic Scattering and Refraction Models for Exoplanet Transit Spectra", **850**, 2, 128 (2017).

Rocchetto, M., I. P. Waldmann, O. Venot, P. O. Lagage and G. Tinetti, "Exploring Biases of Atmospheric Retrievals in Simulated JWST Transmission Spectra of Hot Jupiters", **833**, 1, 120 (2016).

Sagan, C., W. R. Thompson, R. Carlson, D. Gurnett and C. Hord, "A search for life on Earth from the Galileo spacecraft", **365**, 6448, 715–721 (1993).

Schwieterman, E. W., V. S. Meadows, S. D. Domagal-Goldman, D. Deming, G. N. Arney, R. Luger, C. E. Harman, A. Misra and R. Barnes, "Identifying Planetary Biosignature Impostors: Spectral Features of CO and O_4 Resulting from Abiotic O_2/O_3 Production", **819**, 1, L13 (2016).

Schwieterman, E. W., T. D. Robinson, V. S. Meadows, A. Misra and S. Domagal-Goldman, "Detecting and Constraining N_2 Abundances in Planetary Atmospheres Using Collisional Pairs", **810**, 1, 57 (2015).

Seager, S., "The future of spectroscopic life detection on exoplanets", Proceedings of the National Academy of Science **111**, 35, 12634–12640 (2014).

Seager, S. and W. Bains, "The search for signs of life on exoplanets at the interface of chemistry and planetary science", Science Advances **1**, 2, e1500047–e1500047 (2015).

Seager, S. and D. Deming, "Exoplanet Atmospheres", **48**, 631–672 (2010).

Segura, A., K. Krelove, J. F. Kasting, D. Sommerlatt, V. Meadows, D. Crisp, M. Cohen and E. Mlawer, "Ozone Concentrations and Ultraviolet Fluxes on Earth-Like Planets Around Other Stars", Astrobiology **3**, 4, 689–708 (2003).

Stevenson, K. B., N. K. Lewis, J. L. Bean, C. Beichman, J. Fraine, B. M. Kilpatrick, J. E. Krick, J. D. Lothringer, A. M. Mandell, J. A. Valenti, E. Agol, D. Angerhausen, J. K. Barstow, S. M. Birkmann, A. Burrows, D. Charbonneau, N. B. Cowan, N. Crouzet, P. E. Cubillos, S. M. Curry, P. A. Dalba, J. de Wit, D. Deming, J.-M. Désert, R. Doyon, D. Dragomir, D. Ehrenreich, J. J. Fortney, A. García Muñoz, N. P. Gibson, J. E. Gizis, T. P. Greene, J. Harrington, K. Heng, T. Kataria, E. M. R. Kempton, H. Knutson, L. Kreidberg, D. Lafrenière, P.-O. Lagage, M. R. Line, M. Lopez-Morales, N. Madhusudhan, C. V. Morley, M. Rocchetto, E. Schlawin, E. L. Shkolnik, A. Shporer, D. K. Sing, K. O. Todorov, G. S. Tucker and H. R. Wakeford, "Transiting Exoplanet Studies and Community Targets for JWST's Early Release Science Program", **128**, 967, 094401 (2016).

Suissa, G., J. Chen and D. Kipping, "A HARDCORE model for constraining an exoplanet's core size", **476**, 2, 2613–2620 (2018).

Suissa, G. and D. Kipping, "TRAPPIST-1e Has a Large Iron Core", Research Notes of the American Astronomical Society **2**, 2, 31 (2018).

Tian, F., K. France, J. L. Linsky, P. J. D. Mauas and M. C. Vieytes, "High stellar FUV/NUV ratio and oxygen contents in the atmospheres of potentially habitable planets", Earth and Planetary Science Letters **385**, 22–27 (2014).

Trotta, R., "Bayes in the sky: Bayesian inference and model selection in cosmology", Contemporary Physics **49**, 2, 71–104 (2008).

Turbet, M., E. Bolmont, J. Leconte, F. Forget, F. Selsis, G. Tobie, A. Caldas, J. Naar and M. Gillon, "Modeling climate diversity, tidal dynamics and the fate of volatiles on TRAPPIST-1 planets", **612**, A86 (2018).

Unterborn, C. T. and W. R. Panero, "The Effects of Mg/Si on the Exoplanetary Refractory Oxygen Budget", **845**, 1, 61 (2017).

Wolf, E. T., "Assessing the Habitability of the TRAPPIST-1 System Using a 3D Climate Model", **839**, 1, L1 (2017).

Wunderlich, F., M. Godolt, J. L. Grenfell, S. Städt, A. M. S. Smith, S. Gebauer, F. Schreier, P. Hedelt and H. Rauer, "Detectability of atmospheric features of Earth-like planets in the habitable zone around M dwarfs", **624**, A49 (2019).

Zechmeister, M., S. Dreizler, I. Ribas, A. Reiners, J. A. Caballero, F. F. Bauer, V. J. S. Béjar, L. González-Cuesta, E. Herrero, S. Lalitha, M. J. López-González, R. Luque, J. C. Morales, E. Pallé, E. Rodríguez, C. Rodríguez López, L. Tal-Or, G. Anglada-Escudé, A. Quirrenbach, P. J. Amado, M. Abril, F. J. Aceituno, J. Aceituno, F. J. Alonso-Floriano, M. Ammler-von Eiff, R. Antona Jiménez, H. Anwand-Heerwart, B. Arroyo-Torres, M. Azzaro, D. Baroch, D. Barrado, S. Becerril, D. Benítez, Z. M. Berdiñas, G. Bergond, P. Bluhm, M. Brinkmöller, C. del Burgo, R. Calvo Ortega, J. Cano, C. Cardona Guillén, J. Carro, M. C. Cárdenas Vázquez, E. Casal, N. Casasayas-Barris, V. Casanova, P. Chaturvedi, C. Cifuentes, A. Claret, J. Colomé, M. Cortés-Contreras, S. Czesla, E. Díez-Alonso, R. Dorda, M. Fernández, A. Fernández-Martín, B. Fuhrmeister, A. Fukui, D. Galadí-Enríquez, I. Gallardo Cava, J. Garcia de la Fuente, A. Garcia-Piquer, M. L. García Vargas, L. Gesa, J. Góngora Rueda, E. González-Álvarez, J. I. González Hernández, R. González-Peinado, U. Grözinger, J. Guàrdia, A. Guijarro, E. de Guindos, A. P. Hatzes, P. H. Hauschildt, R. P. Hedrosa, J. Helmling, T. Henning, I. Hermelo, R. Hernández Arabi, L. Hernández Castaño, F. Hernández Otero, D. Hintz, P. Huke, A. Huber, S. V. Jeffers, E. N. Johnson, E. de Juan, A. Kaminski, J. Kemmer, M. Kim, H. Klahr, R. Klein, J. Klüter, A. Klutsch, D. Kossakowski, M. Kürster, F. Labarga, M. Lafarga, M. Llamas, M. Lampón, L. M. Lara, R. Launhardt, F. J. Lázaro, N. Lodieu, M. López del Fresno, M. López-Puertas, J. F. López Salas, J. López-Santiago, H. Magán Madinabeitia, U. Mall, L. Mancini, H. Mand el, E. Marfil, J. A. Marín Molina, D. Maroto Fernández, E. L. Martín, P. Martín-Fernández, S. Martín-Ruiz, C. J. Marvin, E. Mirabet, P. Montañés-Rodríguez, D. Montes, M. E. Moreno-Raya, E. Nagel, V. Naranjo, N. Narita, L. Nortmann, G. Nowak, A. Ofir, M. Oshagh, J. Panduro, H. Parviainen, J. Pascual, V. M. Passegger, A. Pavlov, S. Pedraz, A. Pérez-Calpena, D. Pérez Medialdea, M. Perger, M. A. C. Perryman, O. Rabaza, A. Ramón Ballesta, R. Rebolo, P. Redondo, S. Reffert, S. Reinhardt, P. Rhode, H. W. Rix, F. Rodler, A. Rodríguez Trinidad, A. Rosich, S. Sadegi, E. Sánchez-Blanco, M. A. Sánchez Carrasco, A. Sánchez-López, J. Sanz-Forcada, P. Sarkis, L. F. Sarmiento, S. Schäfer, J. H. M. M. Schmitt, P. Schöfer, A. Schweitzer, W. Seifert, D. Shulyak, E. Solano, A. Sota, O. Stahl, S. Stock, J. B. P. Strachan, T. Stuber, J. Stürmer, J. C. Suárez, H. M. Tabernero, M. Tala Pinto, T. Trifonov, G. Veredas, J. I. Vico Linares, F. Vilardell, K. Wagner, V. Wolthoff, W. Xu, F. Yan and M. R. Zapatero Osorio, "The CARMENES search for exoplanets around M-dwarfs. Two temperate Earth-mass planet candidates around Teegarden's Star", **627**, A49 (2019).